Universidade de Lisboa
Faculdade de Ciências
Departamento de Química e Bioquímica

Protein-monolayer interactions investigated by fluorescence microscopy and correlation spectroscopy

Alena Khmelinskaia

Dissertação
Mestrado em Bioquímica
(Bioquímica)

2013

Universidade de Lisboa
Faculdade de Ciências
Departamento de Química e Bioquímica

Protein-monolayer interactions investigated by fluorescence microscopy and correlation spectroscopy

Alena Khmelinskaia

Dissertação
Mestrado em Bioquímica
(Bioquímica)

Tese orientada por

Dr. Grzegorz Chwastek, Max-Planck-Institute for Biochemistry, Munique

Dr. Ana Coutinho, Faculdade de Ciências, Universidade de Lisboa

2013

“What are you working on?” Mr. K. was asked. Mr. K. replied: “I’m having a hard time; I’m preparing my next mistake.”

Stories of Mr. Keuner by B. Brecht

FORWARD

The described project was developed in the Cellular and Molecular Biophysics Department, headed by Prof. Petra Schwille, in the Max-Planck-Institute for Biochemistry, Martinsried (near Munich), Germany. The experiments were conducted under the supervision of Dr. Grzegorz Chwastek, in the period between 15th August 2012 and the date of submission. All the described data was acquired by the author.

During this period, the group moved from its former location in Biotechnologisches Zentrum, TU Dresden, Germany to its current location in Martinsried.

Dr. Ana Coutinho was the internal supervisor, in name of the Faculty of Science, University of Lisbon, Portugal.

ACKNOWLEDGEMENTS

To Petra Schwille for the given opportunity to join this exciting group in one of its most challenging moments, the provided amazing technical support and the sponsored conferences;

To my supervisor Grzesiek for the guidance and teaching, the freedom and the first steps of independence, the support and the fun... for being a bossy friend and a friendly boss;

To Ana Coutinho, my internal supervisor, for being always ready for discussion and for making the bridge with the Faculty of Science in Lisbon;

To all the members of the Cellular and Molecular Biophysics at the Max-Planck-Institute for Biochemistry, present and past, which I had the opportunity to meet, to connect and to grow with, for the amazing year – apart the shared scientific experience, all the social and cultural group activities: the Bavarian Alps discovery, the exhausting Frisbee games, the Tango evenings, the barbeques and parties...

More especially to the Munich 'family': to Henri for the 'Henries', the sofa and the Portuguese soul; to Franzi for the best cakes ever, the company in the endless working nights and the Tahiti dream; to Sonal for the comprehension, the balcony talks and the crazy 'who cares' days; to all three of you for the friendship, the discussions and the (psychological) support;

To Rodrigo for the introduction to the 'membrane biophysics' world, the encouragement, support and discussions, the happy welcome in every return and the friendship that remains;

To Miguel for keeping my feet on the earth and the sky above the head;

To my friends who make Lisbon my other home;

To my family, most especially to my mom Elena and Pedro, the ones who keep me in motion through the hardest days;

To all of you,

Dankeshön!

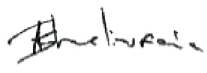

RESUMO

A membrana celular é composta por uma ampla variedade de lípidos e proteínas. Através do estabelecimento de interacções entre lípidos e proteínas, quer membranares quer solúveis, podem ser originadas heterogeneidades espaciais, levando à formação de 'jangadas lipídicas'. Estes domínios transitórios desempenham um papel fundamental em diferentes cadeias de sinalização celular. Apesar da investigação desenvolvida na área, a membrana celular é ainda hoje um dos componentes celulares menos bem compreendidos.

Nas últimas décadas têm vindo a surgir um conjunto de diferentes metodologias *in vitro* que permitem o estudo de variados processos biológicos sob condições definidas e controladas. Neste sentido, foram desenvolvidos variados modelos membranares minimalistas, como GUVs (*giant unillamelar vesicles*), GPMVs (*giant plasma membrane vesicles*) and SLBs (*supported lipid bilayers*), permitindo a análise das interacções lípido-proteína até a um nível unimolecular. Quando correctamente aplicados estes modelos permitem simplificar o sistema isolando virtualmente o fenómeno ou a partícula de interesse retendo, porém, as suas características fundamentais. Apesar da vantagem evidente do uso destes modelos, estas abordagens experimentais são tediosas, envolvendo geralmente o uso de amostras de elevado volume e em que a variação de certas características membranares (como a difusão lipídica) é apenas possível por alteração da composição lipídica ou da temperatura.

As monocamadas lipídicas são historicamente descritas como o primeiro sistema lipídico observado, formando-se por distribuição espontânea de moléculas lipídicas sobre a interface água - ar e formação de filmes finos sobre superfícies. Dado o seu *design* único, a mobilidade e compactação lipídica podem ser facilmente ajustadas neste sistema modelo por compressão da monocamada depositada na interface. Apesar de o seu uso em ensaios de ligação proteica, este sistema tem sido negligenciado na investigação membranar recente devido à sua restrita aplicação. Mais concretamente, as tinas de Langmuir comercialmente disponíveis não são compatíveis com microscopia confocal, estando assim limitadas à monitorização da pressão superficial (π). Além disso, dado o volume de cada amostra relativamente elevado (cerca de 100 mL), são necessárias elevadas quantidades de proteína purificada, comprometendo assim a sua aplicação em estudos biológicos.

Neste estudo, foi utilizada uma nova tina miniaturizada de área fixa, desenvolvida no grupo por Chwastek (Chwastek & Schwille, 2013). As suas dimensões reduzidas permitem não só o uso de amostras de pequeno volume (cerca de 200 µL) como também conferem a versatilidade necessária para o seu acoplamento a um microscópio confocal. Deste modo, é possível aplicar técnicas de imagiologia de alta resolução (permitindo a eliminação de ruído de fundo, o controlo de profundidade de campo e a compilação de secções ópticas de amostras espessas oferecido pelo microscópio confocal), assim como espectroscopia de correlação de fluorescência (FCS – técnica espectroscópica cuja sensibilidade advém do uso de baixas concentrações de sonda e na consequente medição de flutuações espontâneas da intensidade de fluorescência que resultam de desvios estocásticos do sistema relativamente ao seu equilíbrio térmico).

O objectivo global deste projecto prende-se com a melhor compreensão da interacção estabelecida entre proteínas e monocamadas lipídicas. Mais concretamente foi medida a ligação a monocamadas lipídicas de duas proteínas estruturalmente bem caracterizadas: a estreptavidina – proteína tetramérica solúvel com elevada afinidade de ligação para a biotina ($K_D \approx 10^{-15}$ M); e a toxina da cólera – enterotoxina, secretada pela bactéria *Vibrio cholerae,* constituída por um anel homo-pentamérico de subunidades B ($CtxB_5$), responsável pela sua ligação ao receptor membranar gangliósido G_{M1} ($K_D \approx 10^{-9}$ ou 10^{-10} M), e uma subunidade A com actividade de ribosilação que é parcialmente internalizada pelas células do hospedeiro, perturbando cascatas celulares de sinalização e desencadeando a infecção colérica. Foram realizadosensaios de ligação proteica a monocamadas lipídicas homogéneas e com separação de fases, na ausência ou presença dos respectivos ligandos específicos, de modo a distinguir e caracterizar os diferentes comportamentos proteicos. Em última análise, procurou-se desenvolver e optimizar um ensaio universal e quantitativo de ligação proteica a membranas lipídicas.

Previamente aos estudos das interacções proteína-monocamanda, procedeu-se à caracterização morfológica das monocamadas lipídicas, assim como da mobilidade lipídica, recorrendo a microscopia confocal e a FCS, respectivamente. Observou-se pois que a fluidez e homogeneidade global das monocamadas é acompanhada pelo aumento linear do coeficiente de difusão em função da densidade lipídica no intervalo estudado (50 a 90 *MMA* – área molecular média em $Å^2$), tal como se prevê do modelo de área livre (*free area model*). Mais, os valores obtidos para o ponto crítico do DMPC (36.0 ± 4.7 e 37.2 ± 13.5 $Å^2$ em misturas marcadas com sondas diferentes) encontram-se dentro do erro dos valores descritos na literatura. Apesar da robustez demonstrada pelo sistema, é porém necessário ter em conta a possibilidade de ocorrerem desvios em extremos de densidade lipídica (50 e 100 *MMA*), por formação de fases S (sólida) e G (gás), respectivamente.

Após validação da metodologia proposta, procedeu-se ao estudo da influência da compactação lipídica na ligação proteica à monocamada – quer com a estreptavidina, quer com a $CtxB_5$ observou-se uma preferência para a ligação a monocamadas de baixa densidade lipídica e, correspondentemente baixa π e elevada difusão lipídica. Estes resultados são ainda suportados pelas experiências realizadas em misturas lipídicas com separação de fase – ambas as proteínas apresentam uma elevada afinidade para a fase fluida LE (*liquid expanded*) em comparação com os domínios compactos LC (*liquid condensed*). Adicionalmente, resultados de titulações de monocamadas com $CtxB_5$ apontam para a mesma tendência visto que a 90 *MMA* se obtêm intensidades de fluorescência proteica ao nível da monocamada superiores que a 50 *MMA*. Este comportamento já tinha sido proposto no início da década de 80 tendo por base a análise de variações de π por adição proteica a monocamadas lipídicas (Phillips et al, 1975; Fidelio et al, 1981; Cumar et al, 1982). Porém, no caso da estreptavidina observa-se ainda um comportamento extraordinário de acumulação nas bordas de domínios quando a diferença na organização lipídica entre diferentes fases é muito elevada.

A especificidade de ligação foi apenas possível para a $CtxB_5$ por incorporação de G_{M1} na monocamada. Titulações de monocamadas demonstraram que a presença de uma baixa concentração do gangliósido (0.1 mol %) é suficiente para aumentar fortemente a ligação da proteína à monocamada. Além disso, em sistemas lipídicos homogéneos a proteína retém a

preferência por baixas densidades lipídicas. Porém, na presença de separação de fases, a presença de G_{M1} promove a ligação de CtxB5 a domínios LC, dado que este se incorpora preferencialmente em domínios rígidos.

Apesar da elevada reprodutibilidade associada às medições em lípidos, a aplicação do sistema a proteínas tem um erro associado bastante elevado que impede ainda uma quantificação exacta da sua ligação aos lípidos. É de salientar que para além da elevada sensibilidade do sistema de detecção usado, as monocamadas lipídicas formadas sobre a interface água-ar são altamente sensíveis a diferentes factores externos (p.e. oxidação lipídica, formação de menisco e não homogeneidades da compactação lipídica aquando da deposição lipídica, evaporação da subfase, deposição proteica, etc.) que ainda não são totalmente controladas. Deste modo, é ainda necessário proceder à optimização do método de modo a poder determinar-se K_D da ligação de proteínas à superfície lipídica.

Este projecto resultou pois na obtenção de novos dados semi-quantitativos de que a compactação lipídica desempenha um papel importante na interacção proteína-membrana. A separação de fases surge pois como um mecanismo de regulação da ligação proteica, não só por controlo da mobilidade lipídica mas também por segregação de ligandos.

Em suma, a abordagem aqui proposta surge como uma alternativa poderosa para estudos de interacções membrana-proteina, permitindo o fácil ajuste de parâmetros membranares como a compactação lipídica, difícil de regular em sistemas de bicamadas. A sua combinação potente com a microscopia confocal e espectroscopia de correlação de fluorescência resulta não só numa elevada resolução temporal da mobilidade de partículas lipídicas, como também na alta resolução espacial da ligação proteica. Deste modo, o trabalho apresentado contribuiu para a aproximação ao desenvolvimento de um novo ensaio quantitativo global de ligação proteica a membranas lipídicas.

Palavras-chave: ensaios de ligação proteica, microscopia confocal, FCS, compactação lipídica, monocamadas, interacção proteína-monocamada

ABSTRACT

Cellular membranes are composed of a wide variety of lipids and proteins which can lead to spatial heterogeneity and formation of so-called 'lipid rafts', which play an important role in signaling processes.

To investigate these features of lipid bilayers various *in vitro* models have been developed. Although a variety of experimental assays exist, they very often require large samples volume, are complicated and the membrane features can be varied only by changes in lipid composition or temperature.

Here, a fixed-area miniaturized monolayer trough was used. Due to its unique design, lipid mobility in monolayers is easily accessible while keeping other factors constant. The system utilized in this study allows the use of small sample volumes (200 µL) and can be combined with a confocal microscope and thus providing access to high resolution imaging and sensitive fluorescence correlation spectroscopy (FCS) technique.

The goal of the project was to design a quantitative assay by which protein-monolayer interactions can be studied. Thus, monolayers were investigated in terms of morphology and lipid mobility. Further, interactions of well-known ligand-protein pairs were studied: cholera toxin (Ctx)/ganglioside G_{M1} and streptavidin/biotin. The influences of phase separation and presence of lipid ligands were investigated.

It was shown that the membrane affinities of cholera toxin B ($CtxB_5$) and streptavidin depend on the surface density of lipid molecules. Moreover, FCS measurements indicate a correlation between higher protein binding and increased lipid mobility. When phase separated lipid monolayers were used, both proteins bound preferentially to liquid expanded phase (LE). However, in case of $CtxB_5$, in the presence of the ganglioside, the protein mostly binds to the liquid condensed phase (LC).

In summary, protein binding to lipid monolayers was studied by means of fluorescence microscopy and spectroscopy. During the studies, an appropriate methodology was developed and several experimental scenarios were tested.

Key words: protein binding assay, confocal microscopy, FCS, lipid packing, monolayers, protein-monolayer interaction

CONTENTS

MOTIVATION

The cell is the ‘building block’ of life– from bacteria to higher eukaryotes, cell is the structural and functional unit. It consists of a protoplasm, enclosed within a lipid membrane. At the molecular level, cells are composed of proteins, the so-called 'cellular tools' and nucleic acids known as a 'hereditary database'. From complex networking between these components emerge vital functions, which allow cells to sense and react to changes taking place in the environment. This versatility enables cells to evolve and organize into various organisms, which could successfully survive an evolutionary pressure.

Therefore, a better understanding of the biochemical and biophysical nature of individual components of the cell and their interactions is fundamental for broadening the knowledge of the principles of life. Due to the complexity of biological systems, one has to apply a reductionist approach, by which the system is simplified to such an extent that the component/phenomenon of interest is virtually isolated but still retains its main features.

Cell membrane, especially its organization and the role in fundamental cellular processes, is probably one of the least understood components of the cell. Even though great advancements have taken place in this field of research over the last three decades, interactions between lipid membranes and a variety of integral and peripheral membrane-binding proteins are still far from being fully understood.

GOAL

Thus, the general aim of this project was a better understanding of the interaction of proteins with lipid monolayers. More specifically, the binding of two well-characterized proteins (cholera toxin – Ctx, and streptavidin) to lipid monolayers was measured. A new, miniaturized monolayer setup was used to manipulate lipid packing and to investigate its influence on protein binding to lipid monolayers. Particularly, the project was focused on improvement and development of the monolayer technique by combining it with confocal microscopy and fluorescence correlation spectroscopy. The aim was to make protein-binding assays used in other model membrane systems available to lipid monolayers.

I. THEORETICAL INTRODUCTION

1. CELL MEMBRANE

Since the 20th century, lipid membrane is no longer recognized as a simple physical barrier which separates intracellular and extracellular environments, and defines diverse intracellular organelles (Gennis, 1989), but rather as a sophisticated organelle itself which directly or indirectly participates in a variety of cellular processes such as protein and lipid synthesis, metabolite transport and cell signaling.

Nowadays, scientists focus on the structural diversity of biological membranes, the asymmetry of lipid distribution between membrane leaflets and lateral heterogeneity of lipid bilayers in order to propose a coherent view of the cell membrane, which will cover the major biological aspects of this organelle (de Almeida & Loura, 2004). It is widely accepted that the cell membrane is structurally composed of two lipid leaflets (hence its name – the lipid bilayer) (Gorter & Grendel, 1925). Moreover, it contains almost 50 % w/w of proteins in its lipid core (Singer & Nicolson, 1972) and shows structural and functional heterogeneity, as proposed by the so called 'lipid-raft model' (Simons & Ikonen, 1997) – fig. 1.

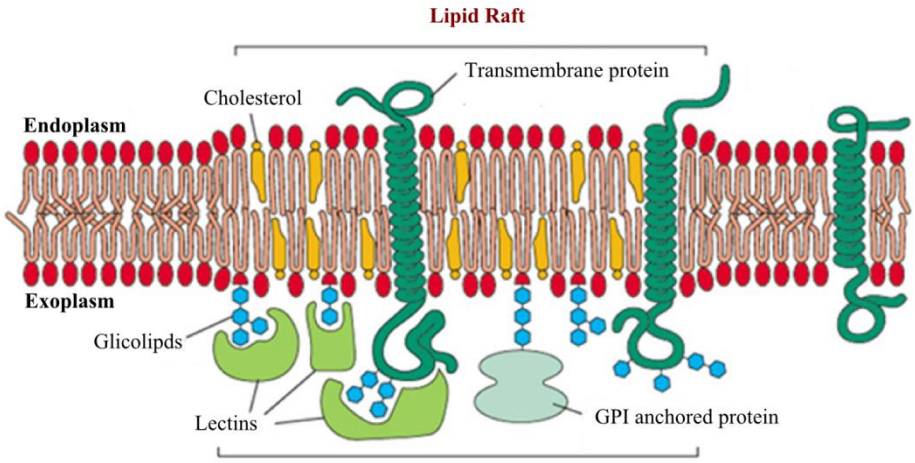

Fig. 1: Schematic representation of the 'lipid-raft' model. (van Meer et al, 2008).

*1.1. PROTEIN INTERACTION WITH LIPID MEMBRANES

Proteins are polymers of amino-acids folded in a unique manner which defines their function and specificity. Several levels of protein organization can be distinguished. At a first level, individual amino-acids are covalently attached through amide linkage forming polypeptide sequences. An amino-acid sequence then folds due to free rotation of the amino and acid groups and consequent interaction between close neighbors (mainly hydrogen bonds) forming secondary motifs (fig. 2.*A*) – α-helix, β-sheet and β-turns. Further folding is driven by hydrophobic forces and stabilized by salt bridges and disulfide bonds, which bring in close proximity distant parts of the sequence (fig. 2.*B*). The overall structure of the protein is therefore dependent on the size, orientation and specific amino-acid sequence, determining

the general function of the protein. While there are plenty of small monomeric proteins, some of these can be used as subunits to form major complex multi-domain structures. In many cases, the subunits preserve their original function and the resulting protein complex exhibits increased functionality (fig. 2.*C*).

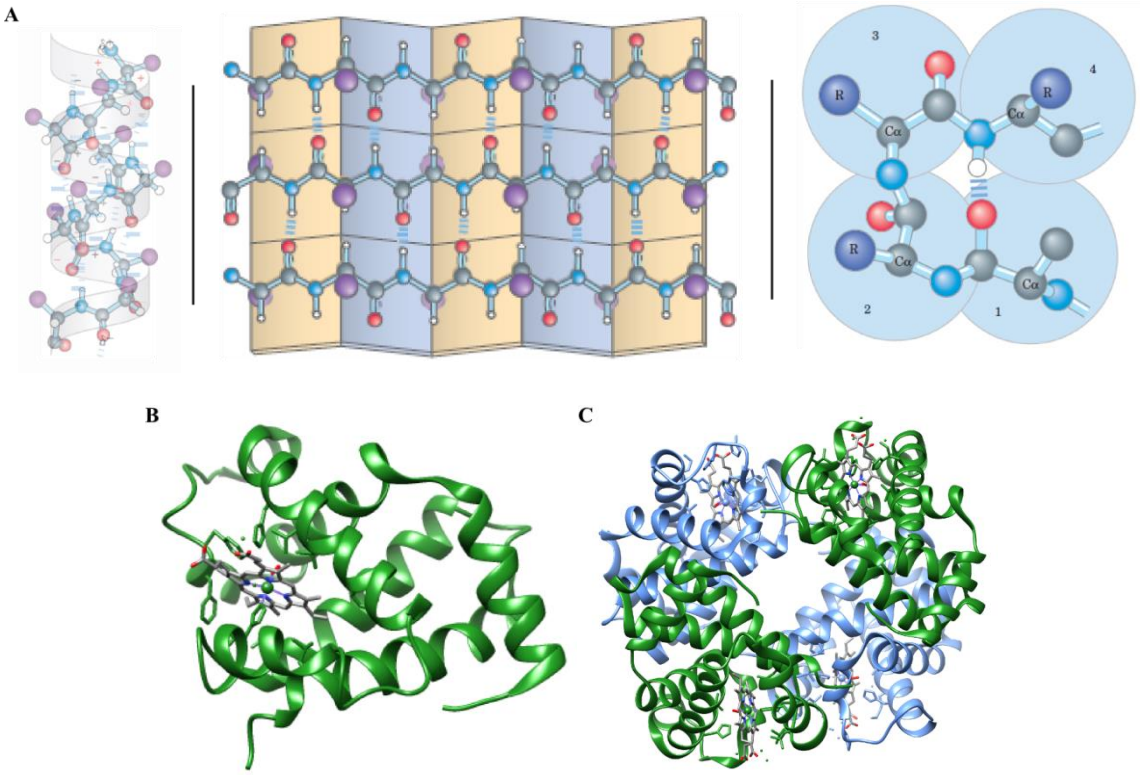

Fig. 2: Levels of protein organization. *A.* Schematic representation of common secondary structure – α-helix (left), β-sheet (center) and β-turn (right). Each ball corresponds to an atom/group in accordance: red – oxygen; blue – nitrogen; black – carbon; white – hydrogen; purple – lateral amino acid group. Dashed lines represent hydrogen bonds. Adapted from (Nelson & Cox, 2004). *B.* 3D representation of hemoglobin *β* subunit tertiary structure. *C.* Quaternary structure of hemoglobin. Blue and green depict *α* and *β* subunit respectively (PDB ID 1GZX).

The wide variety of proteins found in the cell takes part in a complex network of interactions which very often are responsible for the sensing and transduction of signals from and into the cell. Therefore, in the membrane, one can find different sets of integral and membrane-anchoring proteins which facilitate those processes. Integral membrane proteins are embedded in the lipid bilayer through hydrophobic domains such as β barrels or α helix bundles (fig. 3). On the other hand, anchoring proteins are soluble proteins with membrane binding domains which allow them to bind directly or indirectly to the lipid interface.

In nature, a variety of membrane binding domains has evolved and they are an essential part of proteins like protein kinase C (PKC) (Takai et al, 1979), epsin (Ford et al, 2001) and amphiphysin (Lichte et al, 1992). Although different binding domains have the same functionality, the anchoring mechanism to the membrane can be different. For example, plekstrin homology domain (PH) specifically binds to phosphatidylinositol (PI) by amphipatic helixes (Manna et al, 2007) while FYVE domains do it through coordinated zinc ions (Gaullier et al, 1998). Epsin N-terminal homology domain (ENTH) binds specifically to $PI(4,5)P_2$ by positively

charged pockets in its structure (Ford et al, 2001). On the other hand, BAR domains (Bin-Amphiphysin-Rvs) can interact with the membrane through electrostatic interaction (Henne et al, 2007) or anchor to the bilayer through rather hydrophobic amino acid residues (Gallop et al, 2006). Besides the 'specific' nature of membrane-protein interaction, one should take into account rather unspecific interactions raised by the chemical nature of both components.

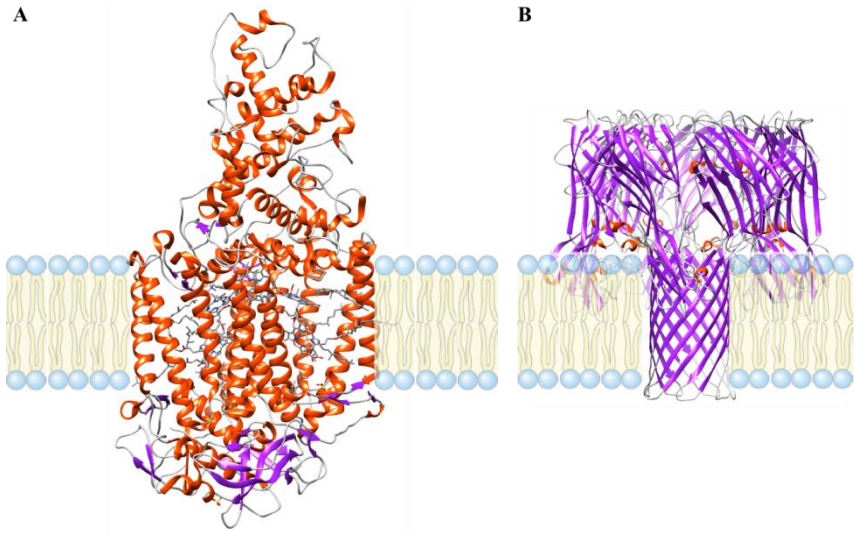

Fig. 3: 3D structure of membrane integral proteins. *A.* Photosyntetic reaction center of Rhodopseudomonas viridis (PDB ID 1PRC) – the membrane binding domain is a bundle of 11 α-helixes. *B. Staphylococcus aureus* hemolysin toxin (PDB ID 7AHL) – the membrane-binding domain is a 14-stranded β-barrel. Addapted from (Nelson & Cox, 2004).

- *1.1.1. CHOLERA TOXIN*

Cholera toxin (Ctx) is the enterotoxin secreted by the bacterium *Vibrio cholerae*, resulting in the massive fluid release characteristic to the cholera infection (Middlebrook & Dorland, 1984). This toxin exhibits a heterohexameric $\alpha\beta_5$ arrangement (Mr = 85.620 kDa) (fig. 4). The five identical *β* subunits ($CtxB_5$) (fig. 4.*A*) which are arranged in a highly stable pentameric ring (Zhang et al, 1995), are responsible for the toxin binding to the cell surface. The natural receptor of the toxin is a sialic acid-containing glycosphingolipid – ganglioside G_{M1} (fig. 5) which is localized on the luminal surface of intestinal epithelial cells (Sattler et al, 1978). The five binding sites are equivalent and have a dissociation constant (K_D) in the order of 10^{-9} / 10^{-10} M (Fishman et al, 1978; Ludwig et al, 1986; Reed et al, 1987). The *α* subunit of Ctx is a loosely folded chain composed of disulfide-linked segments *α1* and *α2* aligned through the central $CtxB_5$ pore that has ADP-ribosilation activity (fig. 4.*C*). The *α* chain is cleaved by bacterial endoprotease prior to internalization (Tomasi et al, 1979) and the *α1* peptide crosses the cell membrane (Mekalanos et al, 1979) and disrupts cell signaling cascades (Holmgren, 1981; Galloway & van Heyningen, 1987; Peterson & Ochoa, 1989).

Therefore, $CtxB_5$ binding to G_{M1} is widely studied as a model of multivalent lipid-protein binding (e.g. Shi et al, 2007; Sorre et al, 2009). The specificity of the interaction also allows the use of $CtxB_5$ as a tool in G_{M1} distribution studies in different lipid membrane models (e.g. Rock et al, 1991; de Almeida et al, 2005). Additionally, due to apparent preferential distribution of G_{M1} into ordered phases (Vié et al, 1998; Yuan & Johnston, 2000; Menke et al, 2002) cholera

toxin is used as a lipid raft marker (e.g. de Almeida et al, 2005; Schafer & Marrink, 2010; Stefl et al, 2012).

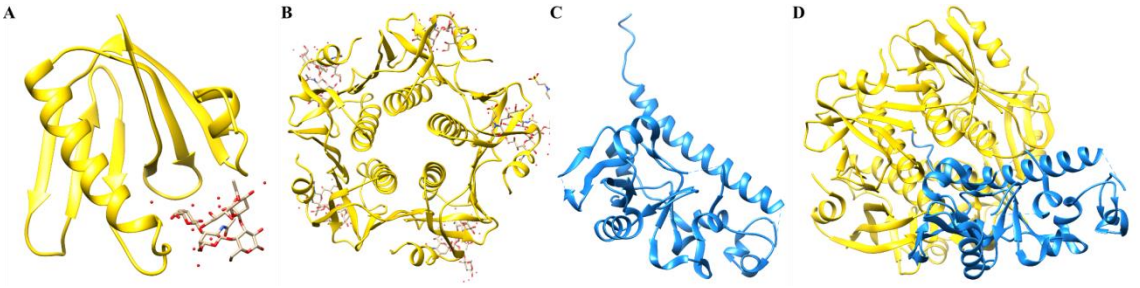

Fig. 4: Cholera toxin (Ctx) 3D structure. *A.* Binding of *β* subunit to membrane ligand G_{M1}. *B.* Ctx membrane binding domain – pentameric $CtxB_5$ ring complex with its ligand G_{M1}. (PDB ID 3CHB) *C.* Ctx enzymatically active *α* subunit. *D.* The *α* subunit aligns through the pore formed by the pentamerc *β* ring. (PDB ID 1S5B)

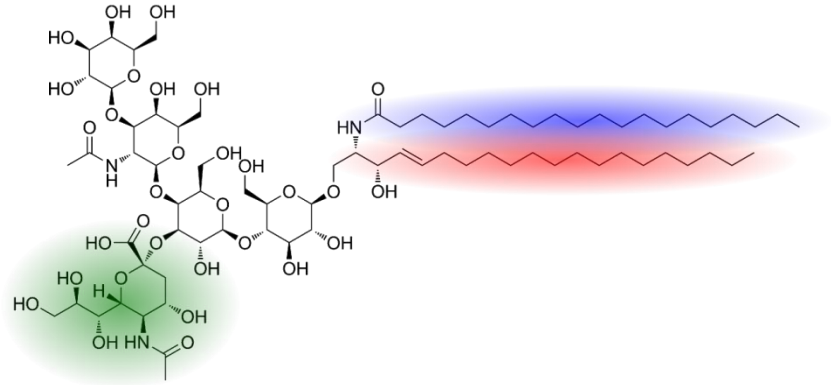

Fig. 5: Strucutre of the ganglioside G_{M1}. – glycoshpingolipid (red – shpingosine; blue – stearic acid) containing four netral sugars and a negatively charged stearic acid (green).

- *1.1.2. STREPTAVIDIN*

Streptavidin, the bacterial equivalent of the hen egg-white protein avidin, is a tetrameric protein (fig. 6) with extraordinary ligand binding affinity (Kd ≈ 10^{-15} M) (Chaiet & Wolf, 1964) to biotin (fig. 7). Each monomer is folded in a simple *β*-barrel structure (fig. 6.*A*) with eight strands in a right-handed helical course and it is stabilized through hydrogen-bonds (Hendrickson et al, 1989). The quaternary structure with dihedral D_2 molecular symmetry arises from intermolecular hydrophobic interactions between specific segments of *β*-strands in each monomer. Biotin binds streptavidin quite deeply in the barrel and only carboxylate oxygens and ureido-ring nitrogen protrude to the outside. Carboxylate groups of biotins bound

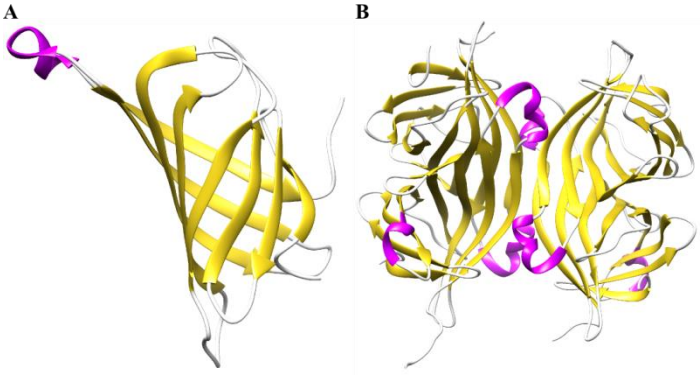

Fig. 6: Streptavidin 3D structure. A. Individual subunits present a simple *β*-barrel conformation. B. Tetrameric structure of streptavidin. (PDB ID 3RY1)

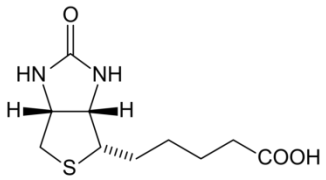

Fig. 7: Streptavidin natural ligand – biotin.

in neighbouring streptavidin subunits are separated by a constant distance of ≈ 20 Å. This structural characteristic might impose a limit to the nature of conjugating groups used in different binding assays. Many evidences from the native X-ray structure and different point mutation approaches suggest that biotin binding is stabilized by numerous van der Waals interactions and hydrogen-bonds evolving the numerous tryptophan residues buried in the barrels (e.g. Hendrickson et al, 1989; Sano & Cantor, 1995; Hyre et al, 2006).

The biological function of streptavidin and avidin is poorly understood and most of the studies on these proteins are performed for a better understanding of the chemical basis of the extreme avidity for biotin and its exploitation in several biotechnological applications, as well as their optimization (e.g. Diamandis & Christopoulos, 1991; Livnah et al, 1993; Nordlund et al, 2003; Laitinen et al, 2007; Vogel & Schwille, 2012; Heinemann et al, 2013).

2. LIPID SYSTEMS FOR *IN VITRO* STUDIES

In the last few decades, a number of *in vitro* methods have been developed that allow the investigation of different biological processes under defined and controlled conditions. A variety of minimal membrane systems (reviewed in Arumugam et al, 2011), as giant unilamellar vesicles (GUVs) (Angelova & Dimitrov, 1986; Merkle et al, 2008; Herold et al, 2012), supported lipid bilayers (SLBs) (Tamm & McConnell, 1985; Chiantia et al, 2006) and lipid monolayers (Fidelio et al, 1981; McConnell et al, 1984; Bianco et al, 1989; Brockman, 1999), allow the study of lipid-protein interactions down to a single-molecule level. These systems, though highly simplified in their composition and topography, when properly employed, retain the core of the interaction under investigation and minimize the number of variables in the analysis.

* 2.1. LIPID ORGANIZATION

Lipids are a broad group of naturally occurring molecules which include fats, waxes, sterols, vitamins, mono-, di- and triglycerides and phospholipids. The major components of lipid membranes are phospholipids and sterols (fig. 8). The exact composition of the lipid bilayer is not only greatly variable between species, but it can be also specific to particular tissues in the same organism and even asymmetric between both leaflets of the same lipid bilayer.

Membranes are formed by spontaneous self-organization of lipid molecules. Due to their amphipathic nature – these molecules have one polar group which coordinates preferentially with the water (hydrophilic) and one non-polar group (fig. 8), which is buried in the hydrophobic core of the bilayer. The character of the lipid molecule depends therefore on the balance between hydrophobic and hydrophilic moiety of the lipid. Hence a common way to characterize lipids is through the determination of the partitioning coefficient of a particular lipid in between oil-water suspension.

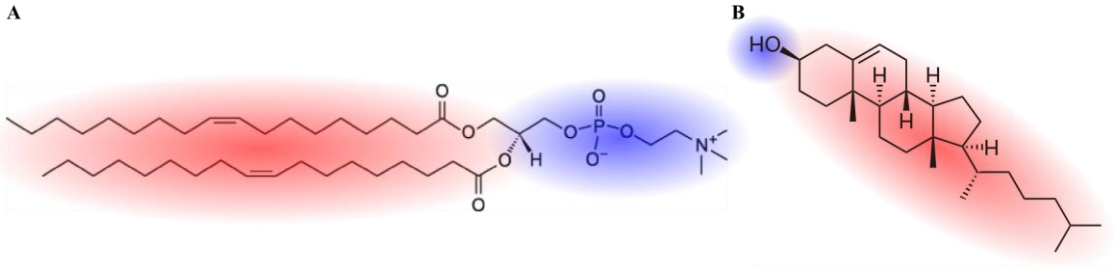

Fig. 8: Structure of representative molecules of common membrane lipid groups – *A.* DOPC (phospholipid) and *B.* Cholesterol (sterol). Lipid amphipathic nature is depicted by different colors – red for hydrophobic regions and blue for polar areas.

Besides the amphipathicity of lipid molecules, another factor playing an important role in the membrane assembly is a theoretical lipid shape. It is called 'shape factor' *S* and it depends on molecule dimensions as well as on the chemical nature of the headgroup, according to:

$$S = V/A_0 L_C \qquad \text{(eq. 1)}$$

where *V* is the volume of the molecule, A_0 is the 'optimal' area of the lipid headgroup taking into account its dimensions and chemical properties of the molecule and L_C is the length of the straight acyl chain. Pure lipids of different shapes form spontaneously different phases (fig. 9): when $S > 1$ (conical shape) the inverted H_{II} phase is favorable (inverted micelle); for $S = 1$ (cylindrical shape), lamellar structures as bilayers are formed; when $S < 1$ (inverted conical shape) micelles are formed. A_0 parameter is mostly dependent on the molecules charge, which can change with the protonation state of the head group. Hence it is directly related to the pH. On the other hand, in case of phospholipids, the L_C and A_H parameters are mainly dependent on the saturation of the acyl chains. In nature, membranes are formed by a wide variety of lipid species of different shape factors. Therefore, it is plausible to form lamellar structures by compensation of conical shapes of one lipid species by the inverted conical shape of another, resulting in a net S ~ 1.

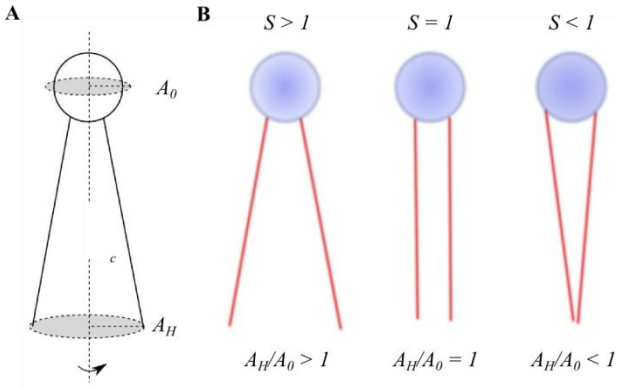

Fig. 9: Lipid structure features. *A.* Schematic orientation of A_0, A_H and L_c parameters relatively to the lipid molecule. *B.* Representation of lipids with different shape factor *S* – cone shaped (left), cylindrical shape (center) and inverted cone shape (right). (Chwastek, 2013)

The properties of the lamellar phase formed by lipids are temperature dependent. Thus, it is possible to distinguish different lipid organizational order, so called 'phases' (fig. 10) – fluid or liquid disordered (l_d), gel phase or ordered solid (gel) and liquid ordered phase (l_o). Under

physiological conditions, the most representative phase of biological membranes is the l_d phase. The bilayer in this phase is relatively thinner and lipid molecules show high lateral mobility. Lipid chains are mostly in a *gauche* conformation or have *cis*-double bonds which lead to a less tight packing in the plain of the membrane and an apparent shortening of the acyl chains (de Almeida & Loura, 2004). With the lowering of the temperature, at certain point (called phase transition temperature - T_m), lipids undergo change in their packing which results in an abrupt reduction of the acyl chain mobility. The highest order of lipid takes place in the so-called gel phase. In this phase, the thickness of the membrane is maximal and lipids are tightly packed due to the presence of ordered acyl chains in *trans* conformation. This leads to almost complete arrest of lateral lipid diffusion. The intermediate l_o phase, on the other hand, though it is characterized by a high lipid order, still retains lipid diffusion (Chiantia et al, 2006). In contrast to gel and l_d phases that are found for all pure lipids, l_o phase is characteristic of mixed bilayers, especially those containing sterols. Generally, this phase forms domains, so called 'lipid rafts', in a l_d matrix. There is a growing number of evidence pointing towards the biological importance of this phenomenon, especially as an important mechanism in the regulation of signaling pathways in the cell (Simons & Ikonen, 1997).

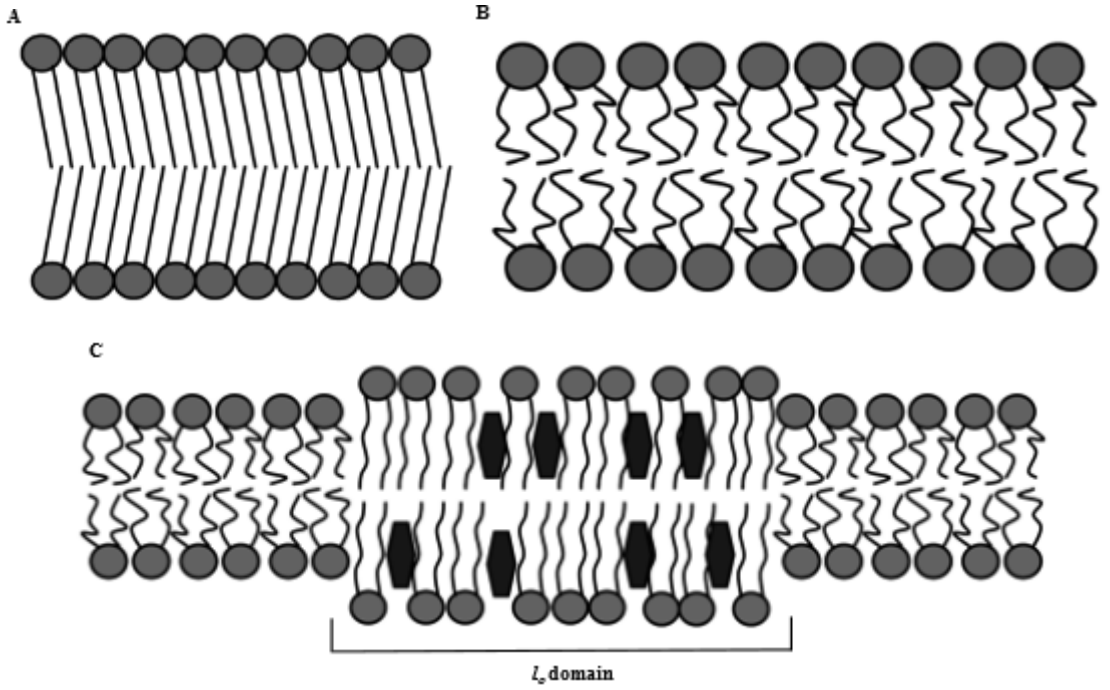

Fig. 10: Schematic representation of different membrane phases – *A.* gel, *B.* l_d and *C.* l_o phases. Adapted from (Franquelim, 2012).

* 2.2. LIPID MONOLAYERS

Historically, lipid monolayers are described as the first lipid systems which originate from the natural lipid spreading at the water-air interface and thin layer formation over available surfaces (reviewed in Dynarowicz-Latka et al, 2001). The major advances in the field occurred during the 19th century: Irving Langmuir studied the surface pressure dependence on molecular density of individual lipids at the water-air interface and, with Katherine Blodgett, developed the lipid film transfer method on to solid surfaces – Langmuir-Blodgett (LB) films. Despite the technological and scientific advances which took place in the field in the 20th

century, the principle of the method remains the same – molecules with amphipathic properties, when deposited on a water-air interface, spontaneously orient themselves in a way that minimizes the overall energy of the system, i.e. the more hydrophilic part of the molecule coordinates with the water subphase whereas the hydrophobic part sticks out towards the air (fig. 11).

Modern Langmuir-Blodgett troughs are composed of a polytetrafluoroethylene (PTFE) container, movable barriers and a micro-balance (fig. 12). The surface pressure (π) is measured through a thin plate of platinum or ash-free filter paper (called Wilhelmy plate) attached to the micro-balance and immersed in the subphase (Martin & Szablewski, 2004). When the π of the monolayer varies, the Wilhelmy plate is exposed to the corresponding force (F) given by equation 2, generated by the surface tension (ST) change due to rearrangement of lipid packing:

$$F = (\rho_P lwt)g - (\rho_L dwt) + 2(w + t)(ST)cos\theta \qquad \text{(eq. 2)}$$

where ρ_P and ρ_L are respectively the plate and subphase densities, $l/w/t$ (length/width/thickness) are the plate dimensions, dwt (where d is the depth of immersion) are the upthrust volume (fig. 13), g represents the gravity and the last term describes the change in ST. Since π is the change in surface tension and the sum of both these parameters is constant, it is thus possible to follow π variation.

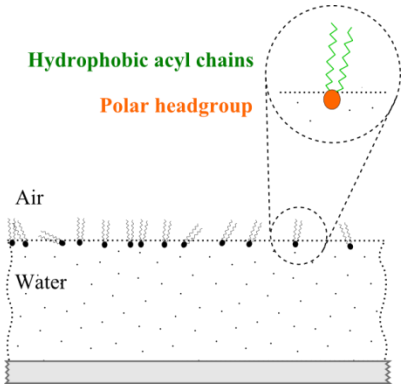

Fig. 11: Schematic representation of lipid deposition on an air-water interface, forming a lipid monolayer. Subphase water molecules penetrate the monolayer to some extent coordinating with the polar headgroups. The hydrophobic acyl chains are completely excluded from water subphase sticking out towards the air. (Chwastek, 2013)

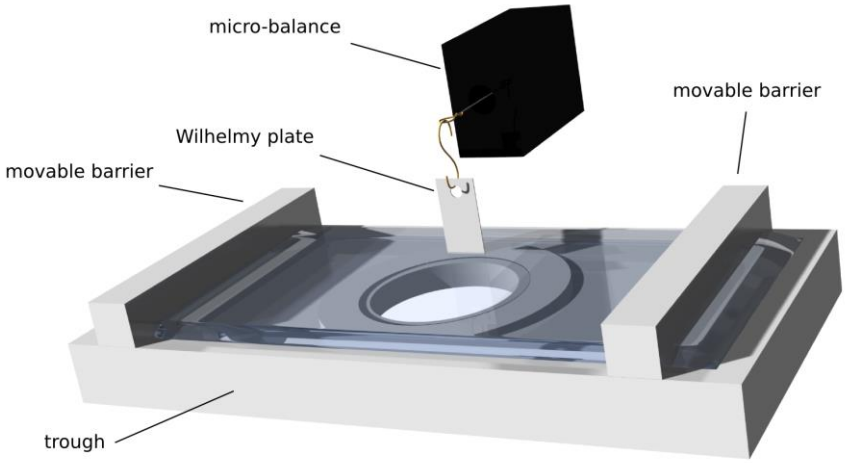

Fig. 12: 3D schematic representation of a classical Langmuir-Blodgett trough with its main components. (Chwastek, 2013)

Thus, knowing that *ST* in standard conditions is 72.8 mN/m, it is possible to calculate π. As the weight plate and the upthrust (first and second term respectively) are constant during the measurement and Θ (contact angle of the subphase to the plate) is 0 ° for Wilhelmy plates, eq. 2 can be simplified to eq.3:

$$F = PlatePerimeter \cdot ST \qquad \text{(eq. 3)}$$

Although the system lacks essential features of a biological membrane, it enables a fine tuning of parameters hardly accessible for a constant lipid composition in bilayer assays – such as lipid packing and surface pressure – which are of great relevance for every lipid-protein interaction. Despite the validation of lipid monolayers in protein binding assays (Brockman, 1999), this classical model system has rather been neglected in recent membrane research due to its restricted applications. Importantly, most of the commercially available troughs are not compatible with confocal microscopes, being limited to π monitoring. On the other hand, the relatively big subphase volume needed for each monolayer experiment (≈ 100 mL) demands huge amounts of purified protein, which renders the applicability in biological studies. Despite the possibility of overcoming these problems through LB films usage, their properties might be influenced by both the solid support and the transfer process.

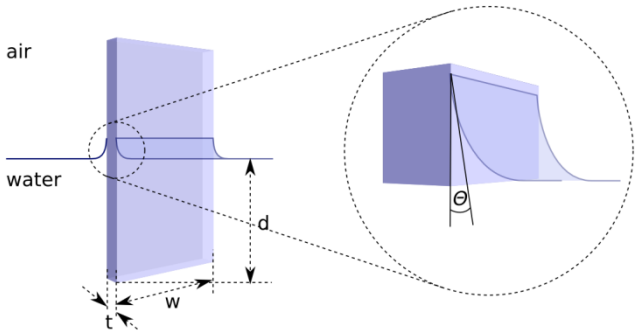

Fig. 13: Schematic representation of Wilhelmy plate – its dimensions and contact angle with the subphase. (Chwastek, 2013)

* 2.3. NEW MINIATURIZED SYSTEM

Very recently, Chwastek and Schwille proposed a small and versatile monolayer setup which allows the combination of confocal microscopy and fluorescence correlation spectroscopy with lipid monolayers (fig. 14) (Chwastek & Schwille, 2013).

This setup is constituted of a PTFE spacer, with a hole of 15 mm diameter, glued to a glass cover slip. A small volume of subphase (≈ 200 µL) is added to the chamber on top of which defined volumes of chloroform lipid solutions are deposited and form lipid monolayers (see Methods; fig. 15). This small chamber volume renders it useful for application in protein-binding assays as well, in which only limited amount of material is available. On the other hand, in contrast to standard monolayer technique, where π measurement is performed, the physical state of the monolayer is monitored by measurement of the diffusion coefficient (*D*) through fluorescence correlation spectroscopy (FCS) (see section 3.3. and Methods). This parameter is commonly used to characterize lipid packing in model membrane systems (Kahya et al, 2003; Chiantia et al, 2009). In monolayers, it has been theoretically predicted (Galla et al, 1979) and experimentally shown (Gudmand et al, 2009) that *D* varies linearly with the mean

molecular area (*MMA*) of lipids in a monolayer far from phase transition, thus allows to control the state of the system.

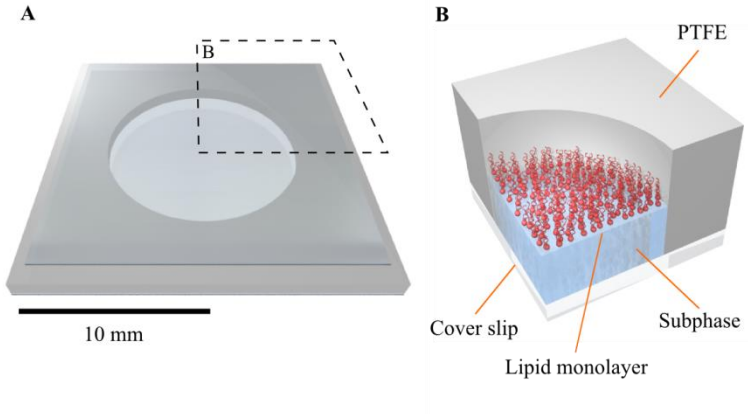

Fig. 14: 3D projection of the micro-chamber. *A.* Chamber overview. *B.* Enlarged schematic representation of the depicted region in *A*. Basic components are demarked. (Chwastek & Schwille, 2013)

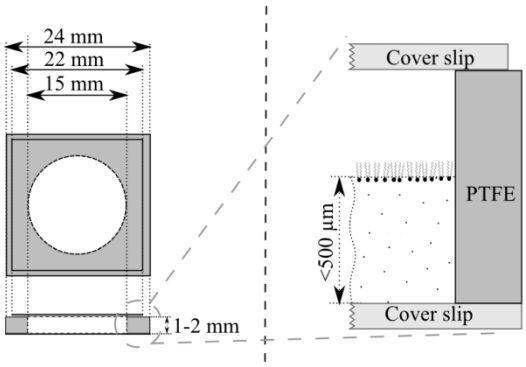

Fig. 15: Schematic representation of the micro-trough for monolayer studies. Chamber components and dimensions are represented relatively to the monolayer. Adapted from (Chwastek & Schwille, 2013).

3. FLUORESCENCE-BASED METHODS

Current biological research is highly focused on the physico-chemical characterization of elementary processes at the level of single molecules. Among techniques used in these studies, highly sensitive and non-invasive fluorescence-based methods are one of the most popular.

* 3.1. FLUORESCENCE

All substances absorb energy in form of light resulting in the excitation of molecules or atoms to a higher quantum state. The spontaneous relaxation to the ground state is accompanied by light emission – luminescence. According to Jablonski's diagram (fig. 16.*A*), depending on the quantum nature of the relaxation phenomena, luminescence can be classified in phosphorescence and fluorescence. Phosphorescence occurs in the millisecond to second time

scale and results from the intersystem crossing conversion (ICC) to the triplet state. Fluorescence, on the other hand, is a much faster process – in the nanosecond regime – which is the result of the relaxation from a singlet excited state to the ground state S_0. (Reviewed in Valeur, 2002; Lakowicz, 2006)

The energy of the emitted photons is in general lower than the absorbed one due to fast non-radiative internal conversion (IC), not only from S_2 to S_1 states but also from higher vibrational states to the ground level of S_1. Moreover, the relaxation often occurs to higher vibrational levels of S_0. This energy loss results in a red shift of the emission spectrum relative to the excitation spectrum known as Stokes' shift (fig. 16.*B*).

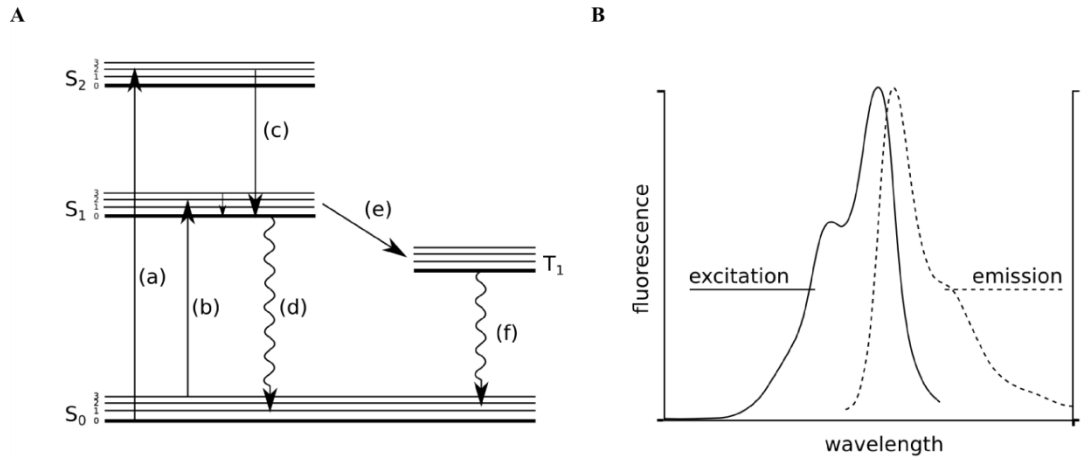

Fig. 16: *A*. Jablonski diagram. Light absorption is accompanied by atom/molecule excitation to one of the vibration levels (depicted by 0, 1, 2 and 3) of the singlet excited states S_1 (b) or S_2 (a). Excited molecules undergo internal conversion (IC) to the ground vibrational level of S_1 (c). From S_1 further relaxation can occur by direct light emission through fluorescence (d) or intersystem crossing conversion (ICC) to the triplet state T_1 I, a much slower process. From T_1, energy is released as phosphorescence. Both phenomena might be therefore distinguished by their lifetime – in the nanosecond time scale for fluorescence compared to the second time scale for phosphorescence. B. Emission and excitation spectra for a fluorophore. The red shift of the emission spectra (Stoke's shift) are due to the energy loss in the non-radiative processes (IC and ICC). (Chwastek, 2013)

The main parameters, which should be considered when using fluorescent probes in biological studies are the absorption cross-section, quantum yield (*Q*) and fluorescence lifetime which should be suitable to the experimental design. The quantum yield is given by the ratio of the number of emitted photons (D_r – rate of S_1 to S_0 decay) to the total number of observed photons ($D_r + D_{non}$, where D_{non} is the rate of all the processes leading to non-radiative energy dissipation) – eq. 4. Fluorescence lifetime is the average time which molecules/atoms stay in the excited state. Moreover, for membrane probing, both *in vivo* and *in vitro*, fluorescent dyes must be amphipathic or hydrophobic in order to incorporate into lipid membranes allowing its characterization. The partition coefficient (K_p) is often used to report probes preference to incorporate into lipid membranes or specific lipid phases.

$$Q = \frac{D_r}{D_r + D_{non}} \qquad \text{(eq. 4)}$$

* 3.2. Confocal microscopy

The basic concept of confocal microscopy was originally developed by Marvin Minsky in the middle of 16th century. In 1979, G. Fred Brakhenhoff developed the first scanning confocal microscope and two decades later appeared the first commercial instruments. Since then, many technological and theoretical advances were made to improve resolution and versatility of confocal microscopes. (Reviewed in Claxton et al, 2005)

Though confocal microscopy provides only a marginal improvement in both axial and lateral optical resolution, the greatest innovation over widefield microscopy is the elimination of out-of-focus light or glare in thick samples (over the immediate plane of focus) through the use of spatial filtering techniques. Thus, the laser beam (excitation source) passes through a pinhole aperture localized in a confocal conjugate plane with the scanning point in the sample and a second pinhole aperture positioned in front of the photomultiplier tube (detector) – fig. 17.*A*. During sample scanning with the laser, reflected by a dichromatic mirror, secondary fluorescence emitted from points on the sample pass back through the dichromatic mirror and are focused as a confocal point at the detector pinhole aperture. As only a small fraction of the out-of-focus emission is delivered through the pinhole aperture, being rather projected onto the aperture as Airy disks. Therefore, most of this extraneous light is not detected by the photomultiplier and does not contribute in the image formation.

Importantly, the focusing mechanism of laser illumination in confocal microscopy also allows reduction the focal volume (fig. 17.*B*) – the laser light is first expanded to fill the objective rear aperture, and then focused by the lens system to a very small point in the focal plane.

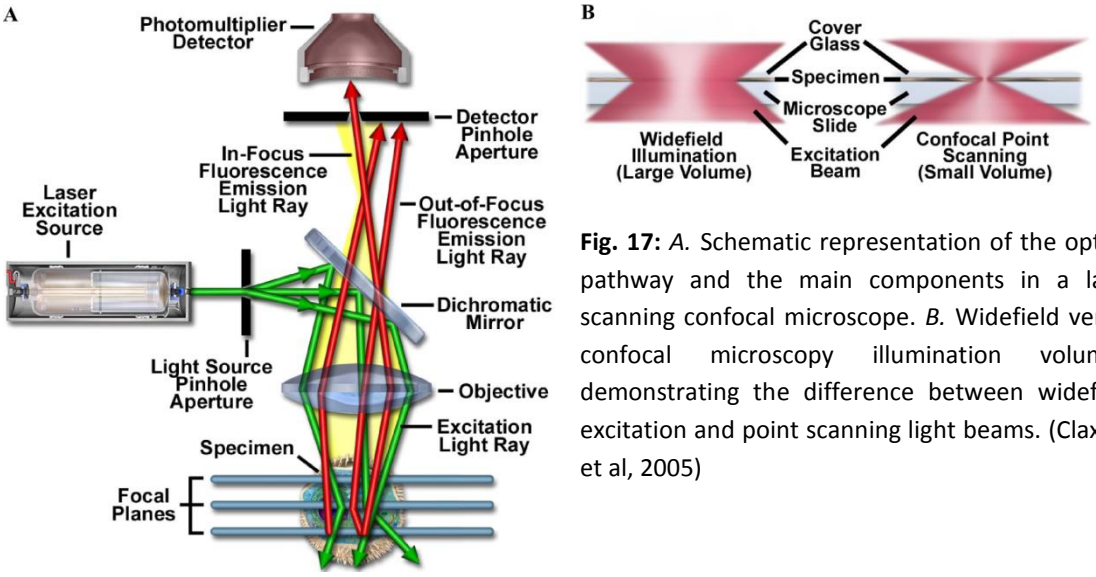

Fig. 17: *A.* Schematic representation of the optical pathway and the main components in a laser scanning confocal microscope. *B.* Widefield versus confocal microscopy illumination volumes, demonstrating the difference between widefield excitation and point scanning light beams. (Claxton et al, 2005)

In laser scanning confocal microscopy the focused beam is scanned across the defined sample area in a raster pattern controlled by two-high speed oscillating mirrors driven with galvanometer motors, allowing for the formation of images of extended samples.

In the whole, confocal microscopy is advantageous over conventional widefield optical microscopy as it offers the ability to control depth of field, to eliminate or highly reduce the background information and to collect serial optical sections from thick samples.

* 3.3. FLUORESCENCE CORRELATION SPECTROSCOPY

Fluorescence correlation spectroscopy (FCS) principle was introduced for the first time by Magde, Elson and Webb in 1972 (Reviewed in Schwille & Haustein, 2002). Unlike other fluorescence techniques, FCS primary parameter of interest is not the fluorescence intensity but rather its fluctuations which appear due to the system stochastic deviations from thermal equilibrium. Therefore, FCS is based on the time correlation of fluorescent signal fluctuations induced by the fluorophore movement in and out of the detection volume (fig. 18). The acquired signal is characteristic to particular particle species and conditions. In order to resolve the movement of single molecules, measurements are usually conducted at very low dye concentration to avoid the saturation of the detection volume. The implementation of confocal detection to the FCS setup by Rigler and co-workers allowed the reduction of the detection volume below one femtoliter (Rigler et al, 1999). The consequent reduction of the average number of detected molecules enables FCS measurement at higher biologically relevant concentrations. Its applicability is nonetheless limited by the resolution scale (> 200 nm) and still sets an upper limit for label concentrations. An alternative arises from the combination of FCS and fluorescence intensity distribution analysis (FIDA) with sub-diffraction-resolution stimulated emission depletion (STED) nanoscopy (Kastrup et al, 2005; Ringemann et al, 2009). This approach, with an effective observational area down to 20-30 nm in diameter (note that the selective deactivation of fluorophores accomplished by double pulse of light enables image enhancement in the region), allows the study of nano-scale dynamics and may be applied to larger, often endogenous concentrations.

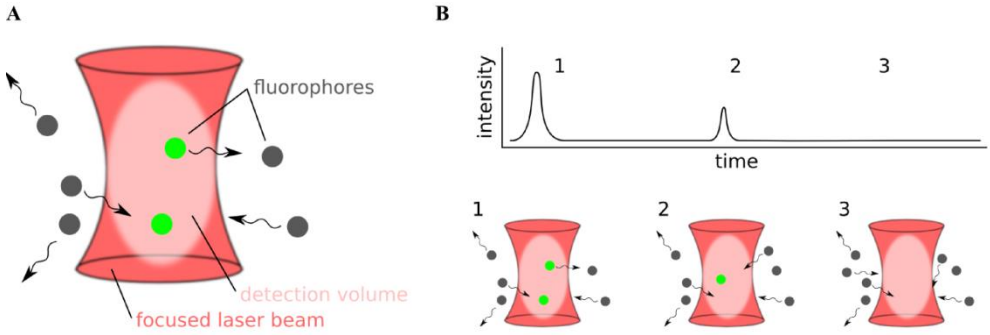

Fig. 18: Principles of fluorescence correlation spectroscopy (FCS). *A.* Fluorophores (grey) diffuse randomly into the focal spot (pink) where the laser beam (red) is strongly focused. Fluorophores start immediately to emit light (green) as a result of the absorbed energy. *B.* Detected signal is directly related to the number of fluorescent molecules in the focal spot. (Numbers at the graph correspond to the numbers at the drawings.) (Chwastek, 2013)

In theory, the fluorescence fluctuations *δF(t)* are deviations from the average fluorescence signal and corresponds to the average number of particles.

$$\delta F(t) = F(t) - < F(t) > \qquad \text{(eq. 5)}$$

Autocorrelation of the signal over time translates the temporal similarity of the signal intensity into its characteristic decay.

$$G(\tau) = \frac{<F(t)\delta F(t+\tau)>}{<F(t)>^2} \qquad \text{(eq. 6)}$$

Assuming that fluorophores undergo Brownian motion, one can conclude that the number of molecules in the focal volume, hence the fluorescence intensity, depends strongly on the mobility of particles. Therefore, fluorophore diffusion determines the characteristic decay of the temporal autocorrelation function.

The detection volume – effective focal volume V_{eff} – is a three dimensional Gaussian approximation (eq. 7), where r_0 is the waist of the focal spot at which the Gaussian approximation of the emitted light decays to $1/e^2$ and z_0 is the dimension along the *z* axis.

$$V_{eff} = \pi^{\frac{3}{2}} \cdot r_0^2 \cdot z_0 \qquad \text{(eq. 7)}$$

The autocorrelation function which describes the diffusion of fluorescent specie has a following form

$$G(\tau) = \frac{1}{V_{eff}<C>}\left(1 + \frac{\tau}{\tau_D}\right)^{-1}\left(1 + \frac{\tau}{\frac{{r_0}^2}{z_0}\tau_D}\right)^{-1/2} \qquad \text{(eq. 8)}$$

where $V_{eff}<C>$ is the average number of molecules $<N>$ in the focal volume and τ_D is the characteristic diffusion time of the fluorescent species. By knowing the diffusion coefficient of the molecule it is possible to estimate the dimension of V_{eff} using the relation:

$$\tau_D = \frac{r_0^2}{4D} \qquad \text{(eq. 9)}$$

Further, by bringing together the number of particles and the estimated detection volume one can extrude the concentration of the fluorophore (eq. 10).

$$G(0) = \frac{1}{<N>} = \frac{1}{V_{eff} \cdot <C>} \qquad \text{(eq. 10)}$$

For a more accurate description of the fluorescence signal fluctuations, besides molecule motion, one needs to consider other fluorescence aspects that might interfere with the measured signal (fig. 19).

The inherent fluorophore blinking due to ICC from S_1 to T_1 interferes with fluctuation arose from lateral mobility of the fluorophore. This phenomenon can be taken into account in the autocorrelation function

$$(\tau) = \frac{1}{<N>}\left(1 + \frac{T}{1-T}e^{-\tau/\tau_T}\right)\left(1 + \frac{\tau}{\tau_D}\right)^{-1}\left(1 + \frac{\tau}{S^2\tau_D}\right)^{-1/2} \qquad \text{(eq. 11)}$$

where *T* corresponds to the triplet fraction, τ_T the diffusion time, *S* is the structural parameter defined by the ratio r_0/z_0 and the triplet blinking is described by an exponential decay (Schwille et al, 2000). This three dimensional model can be also applied to two dimensional situation (like in case of lipid membrane) since S approaches zero:

$$(\tau) = \frac{1}{<N>}\left(1 + \frac{T}{1-T}e^{-\tau/\tau_T}\right)\left(1 + \frac{\tau}{\tau_D}\right)^{-1} \qquad \text{(eq. 12)}$$

As a result the detection volume in this two dimensional model is approximated by a circle allowing to exclude the third term of the 3D model. Notice that thermal instability of the membrane may induce additional fluorescence fluctuation in the 2D situation especially when

applied to free-standing membranes which might move in and out of the focal spot. Thus an additional component describing these fluctuations (*F* fraction with τ_F diffusion time) should be used (Petrov & Schwille, 2008) – eq. 13.

$$(\tau) = \frac{1}{<N>}\left(1 + \frac{T}{1-T}e^{-\tau/\tau_T}\right)\left(\frac{F}{1+\tau/\tau_F} + \frac{1-F}{1+\tau/\tau_D}\right)^{-1} \qquad \text{(eq. 13)}$$

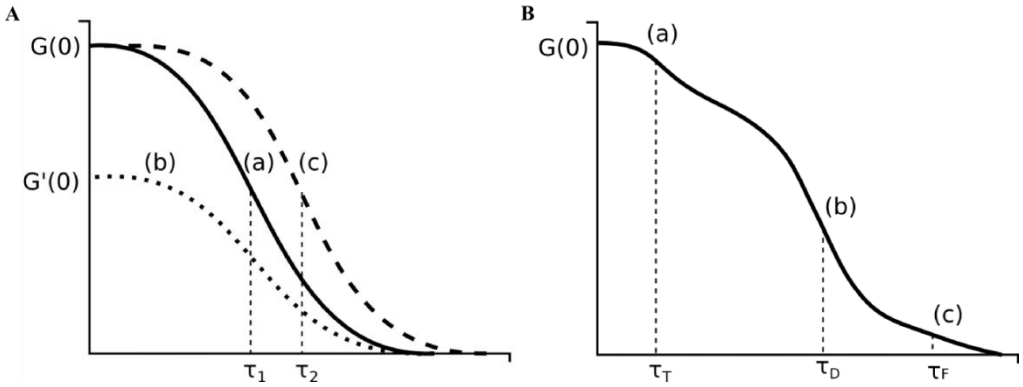

Fig. 19: Influence of different factor on the shape of the autocorrelation curve. *A.* An autocorrelation curve presents characteristic amplitude G(0) and τ_1 diffusion time – (a). In presence of higher concentration of the same fluorophore specie (b), even though the overall signal increases, the amplitude of the correlation drops (G'(0)) accordingly with the equations 8 and 10. Importantly, the characteristic diffusion time is retained. On the other hand, a fluorophore in the same concentration as in (a) but with lower mobility will raise a curve with the same amplitude G(0) but shifted towards longer diffusion times – (c). B. Influence of triplet blinking and membrane undulations – for a fluorophore with a characteristic diffusion time τ_D (b), its triplet state will appear at shorter lag times (τ_T – (a)), as blinking is a much faster process in comparison to lateral diffusion of the molecule; the relatively slow process of membrane undulations will give rise to and additional slow component – τ_F (c). (Chwastek, 2013)

II. MATERIAL AND METHODS

1. MATERIALS

The lipids 1,2-di-(9Z-octadecenoyl)-*sn*-glycero-3-phosphocholine (DOPC – 850375), 1,2-dipalmitoyl-*sn*-glycero-3-phosphocholine (DPPC – 850355), 1,2-dimyristoyl-*sn*-glycero-3-phosphocholine (DMPC – 850345), 1,2-distearoyl-*sn*-glycero-3-phosphocholine (DSPC – 850365), sphingomyelin (bSM – 860062), cholesterol (chol – 700000), ganglioside G_{M1} (860065), 1,2-dipalmitoyl-*sn*-glycero-3-phosphoethanolamine-N-(cap biotinyl) (DPPE-Ncap-Biotin – 870277), 1,2-dioleoyl-*sn*-glycero-3-phosphoethanolamine-N-[methoxy(polyethylene glycol)-350] (DOPE-PEG350 – 880430), 1,2-distearoyl-sn-glycero-3-phosphoethanolamine-N-[biotinyl(polyethylene glycol)-2000] (DSPE-PEG2000-Biotin – 880129) were purchased from Avanti (Alabaster, Al, USA) – catalog numbers given in brackets. Labeled $CtxB_5$ (Alexa 488 – C34775 – and 647 – C34778) and streptavidin (Alexa 488 – S11223), free Alexa 488 (A20000), 546 (A20002) and 647 (A20006), cholesteryl 4,4-difluoro-5-(4-methoxyphenyl)-4-bora-3a,4a-diaza-*s*-indacene-3-undecanoate (Chol 542 – C12680) and 3,3'-dilinoleyloxacarbocyanine perchlorate (DiO – D3898) were purchased from Invitrogen (Carlsbad, CA, USA). In figure 1 are represented the spectra of the dyes used in the main studies. Consumables and machinery are indicated in the next sections.

2. LIPID HANDLING

Lipids were stored at -20 ^{o}C in chloroform (1.02447.0500 – Merck kGaA, Darmstadt, Germany) filled with argon to prevent oxidation and sealed with silicon tape to prevent evaporation. On a daily basis, the lipid concentration was estimated by gravimetric method. Stock solution concentrations which were suspected to be changed over time were determined using Rouser's modified method.

3. ROUSER'S METHOD

This method is based on molibdate ability to form complexes with free phosphorus under acidic conditions. Phospholipids are decomposed into CO_2, H_2O and PO_3^{4-} when incubated at high temperature in perchloric acid. The resulting orthophosphate forms phosphomolybdate (VI) $[(NH_4)_3Pmo_{12}O_{40}]$ in presence of molybdenum ammonium under acidic conditions. This compound is reduced by ascorbic acid to a mixture of molybdenum oxides (IV) and (VI) MoO_2 x MoO_3 – molybdenum blue. The amount of the later is estimated by absorption measurement. Note that this method cannot be used to measure lipid suspensions containing phosphates as all the inorganic phosphorus will contribute for the total mass of measured phosphorus.

Lipids (10 to 100nmols) were pipetted to glass test-tubes. After complete solvent evaporation, 500 µL of water and 300 µL of perchloric acid were added. Short vortexing was proceeded by a 3 hour incubation time at 180 ^{o}C to assure full lipid mineralization and complete phosphorus release.

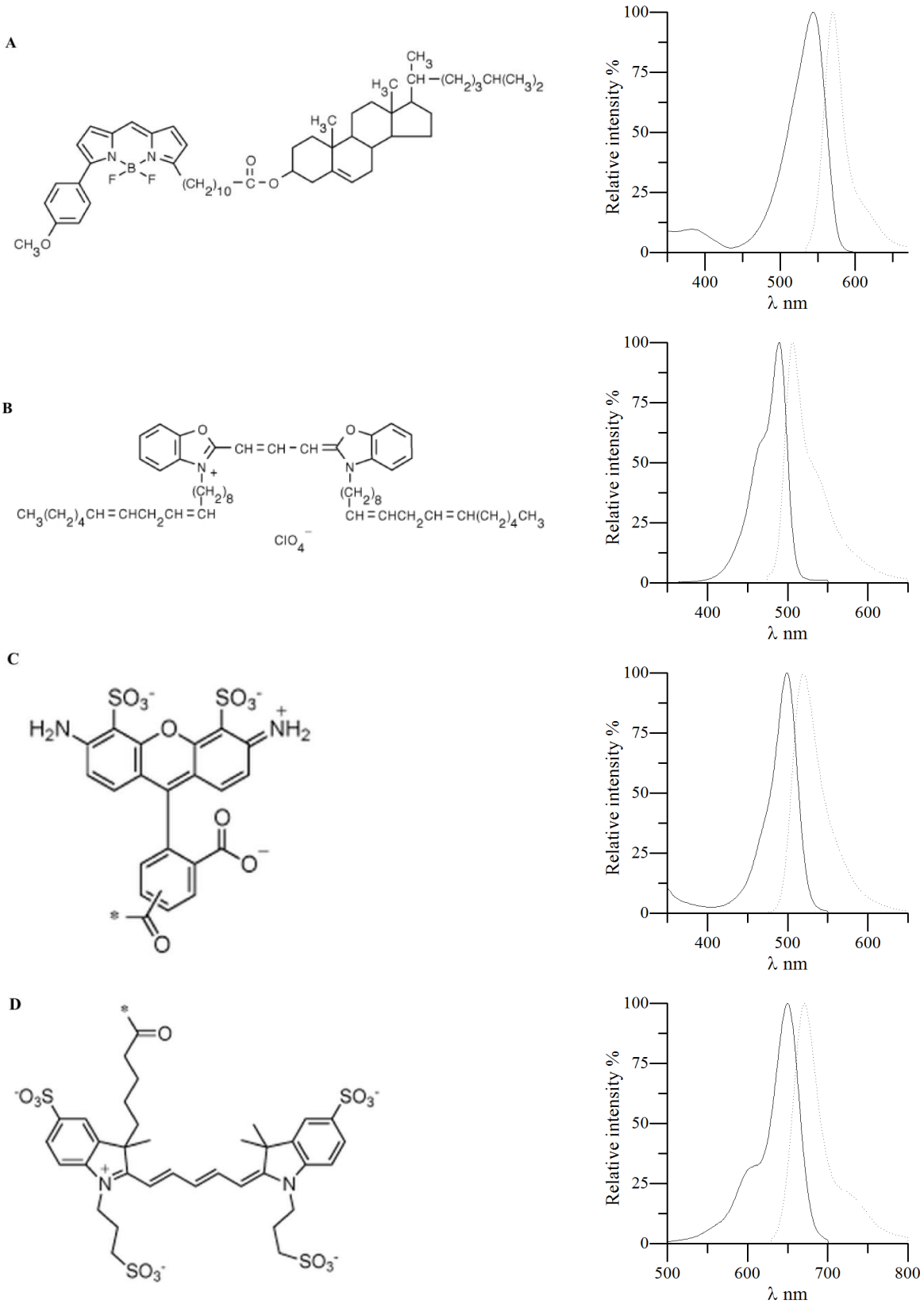

Fig. 1: Chemical structures and optical spectra of the used main fluorescence dyes – Chol 542 (*A*), DiO (*B*), Alexa 488 (*C*) and Alexa 647 (*D*). Spectra with solid line correspond to absorption and dotted line refers do fluorescence emission. * in *C* and *D* marks the connection to the protein. Adapted from www.invitrogen.com

After incubation, test-tubes were cooled down under tap water stream. 2.5 mL of water, 400 µL of ammonium molybdate solution (1.25 % w/v) and 400 µL of fresh ascorbic acid solution (5 % w/v) were added to the test tube. After vortexing, test-tubes were kept at 100 ^{o}C for 15 min.

After cooling down under the tap water stream, absorption at 812 nm was measured with a spectrophotometer (Varian, Cary). Simultaneously with the analyzed samples, a standard curve was prepared, using a phosphorus standard solution instead of lipids.

4. SURFACE PRESSURE (Π) – AREA (A) ISOTHERMS

Standard isotherms were measured using NIMA 112 Langmuir-Blodgett trough equipped with micro-balance. Before use, the trough was thoroughly cleaned with Kimptech paper tissues sequentially soaked in chloroform (C/4960/17 – Fisher Scientific, Leics, UK) and ethanol (32205 – Sigma Aldrich, St. Louis, USA), and dried in between with clean tissue, in three rounds. During the cleaning procedure, powder free gloves were used. Subsequently, the trough was repeatedly (three times) filled with pure water and the water-air interface was vacuum cleaned. A Wilhelmy plate made of ash-free filtration paper was attached to the microbalance and let to soak for 15 min. After reaching the equilibrium, barriers were closed with a speed of 150 cm^2/min and the surface pressure at the air/water interface was monitored. The system was considered ready for use if the surface pressure through the whole closing process (from 80 cm^2 to 25-30 cm^2) would not vary more than 0.3 mN/m. Otherwise, the washing steps would be repeated.

Isotherms of lipid mixtures were measured from a starting zero surface pressure with a compression rate of 5 cm^2/min. The typical lipid concentration was 1 mg/mL. Each lipid mixture was measured at least twice, both on water and on buffer used later for the subphase.

5. MICRO-CHAMBER FOR MONOLAYER STUDIES

Chamber spacers were cut from 2 mm thick sheet of PTFE by a laser cutter (Trotec Laser Inc., Ypsilanti, MI, USA). Glass cover slips 24 x 24 mm^2 with 150 µm thickness (Gerhard Menzel GmbH, Braunschweig, Germany) were fixed to the spacer by glue. Prior to use, chambers were washed interchangeably with ethanol and water, dried with stream of nitrogen and then plasma-cleaned for 10 min, so the glass surface acquires hydrophilic character. For protein assays, the chambers were further incubated with 2 mg/mL bovine serum albumin (BSA) solution for 30 min in order to passivate the glass surface and prevent protein deposition. Buffer filled chambers (200 µL of SLB buffer – 10 nM HEPES (05288.100 – BIOMOL GmbH, Hamburg, Germany), 150mM NaCl (27810.295 – VWR International BVBA, Radnor, Pennsylvania), pH 7.4) were incubated at 40 ^{o}C for 5 min and lipid monolayers were deposited by drop-wise deposition of a chloroform solution of the desired lipid composition on the buffer–air interface (fig. 2.*A*-*B*). The typical lipid concentration was 0.1 mg/mL. After lipid deposition, the sample was covered by a 22 x 22 mm^2 coverslip and allowed to cool down to room temperature (≈ 23 ^{o}C) at least for 5 min. A small volume was removed from the subphase to assure monolayer positioning in the range of the working distance of the objective (fig. 2.*C*-*D*), usually 300 – 600 µm above the cover slip surface. Samples were imaged using a confocal laser scanning microscope (LSM 510, ConfoCor2/3, Zeiss, Jena, Germany) equipped with an LD

C-Apochromat (40x, 1.1 NA) objective with a working distance of 0.62 mm. The focus was placed at the monolayer following laser scattering at the sample interfaces – the first intensity peak corresponds to the water glass-interface (the lower surface of the cover slip); the second to the scattering of the light at the glass-water interface (upper coverslip surface) and the upper reflection corresponds to the buffer-air interface. The right positioning was confirmed by monitoring the fluorescence intensity of the probe incorporated in the monolayer. All image analysis was done using *ImageJ 1.47i*.

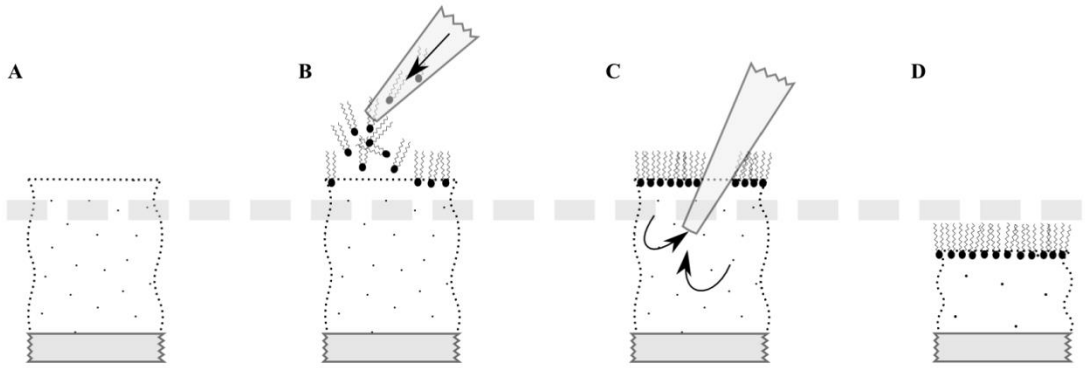

Fig. 2: Schematic overview of the sample preparation. *A.* Subphase addition (200 µL) to the chamber. *B.* Lipid chloroform solution deposition. *C.* Excess subphase volume removal with a pipette. *D.* Ready-to-use sample within the working distance of the objective (thick dashed line). Adapted from (Chwastek & Schwille, 2013).

6. FCS MEASUREMENTS

FCS measurements were performed using LSM 510 ConfoCor 2/3 microsocpe (Zeiss, Jena, Germany). Dichoric 288/543/633 mirror was used as a main beam splitter. Pinholes for APDs (Avalanche Photo Diodes) were set to 72 (for 488 nm laser line), 80 (for 543 nm laser line) and 94 (for 633 nm laser line). Before each measurement the correction ring of the objective (LD C-Apochromat 40x, 1.1 NA, 0.62 mm working distance) was adjusted to maximize the signal and the system pinhole positions were automatically adjusted using GUI, with the focus placed at the monolayer.

For single measurements, 5 second independent traces were averaged (typically 20). Focus correction was necessary over the measurements due to evaporation caused by increased temperature and altered traces were removed from analysis. Data were fitted using Zeiss software after discarding traces over which focus correction was done. Since monolayers are very prone to mechanical instability and inherent undulations due to thermal fluctuations it was necessary to fit a two-component two-dimensional diffusion model with a triplet state (eq. 13) in order to correct for the additional slow component appearing in the correlation curve. Nevertheless, only data in which the slow component was smaller than 5 % were considered. The faster component was used to determine the diffusion time of the lipid dye. In order to calculate the lipid diffusion coefficient, the system was calibrated with Alexa 488 and Alexa 546 dyes which diffusion coefficient are known – 435 $\mu m^2/s$ and 341 $\mu m^2/s$ respectively (Petrasek & Schwille, 2008). In this case, correlation curves were fitted to one component

three dimensional diffusion model with a triplet state (eq. 12) and the focal waist was calculated according to equation 9.

7. PROTEIN BINDING ASSAY

The protein solution (in SLB buffer) was applied by dipping the pipette tip through the monolayer. After 1 min period of incubation the excess added volume was removed by dipping the pipette tip. Protein FCS was measured at the interface as previously described (see FCS measurements)

As FCS data did not allow for proper correlation analysis due to fluctuations in the fluorescence signal originating mainly from protein aggregation upon binding, another approach was used. Count rate obtained during FCS measurement was used as an estimation of the amount of the protein bound to the monolayer and freely diffusing in the solution – eq. 14, where I_F and I_0 represent the intensity of emitted light and the light source respectively, k' is the logarithmic conversion of the geometrical/instrumental factor G, Q is the quantum yield, ε the molar absorptivity, l the sample length and c its concentration.

$$I_F = k' I_0 Q \varepsilon c l \qquad \text{(eq. 14)}$$

For that, it was assumed that the fluorescence collected at the interface has an apparent intensity (C_{app}) as the measured signal has a complex nature. In an ideal case, the focal spot is positioned in such a way that the monolayer is exactly in the middle of the focal spot V_{eff} (fig. 3) so that the upper part is above the monolayer and the lower one is below the interface. Thus, the collected C_{app} is a sum of the signal from the monolayer itself (C_{inter}) and the signal from the lower part of the focal volume, which corresponds to half of the intensity collected in the subphase (C_{sub}). Therefore,

$$C_{app} = C_{inter} + {}^{C_{sub}}/_{2}. \qquad \text{(eq. 15)}$$

Finally, to express protein binding to the monolayer, the ratio C_{inter}/C_{sub} was used.

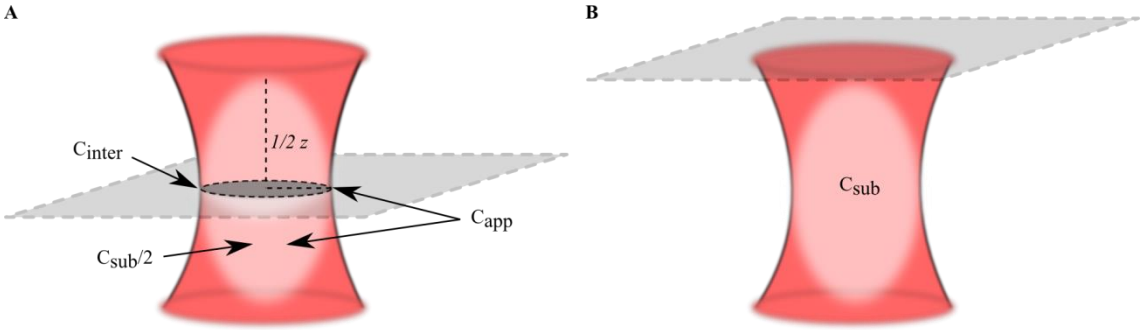

Fig. 3: Schematic representation of V_{eff} positioning in relation to the monolayer (grey). *A.* When the focal spot is positioned at the interface, ideally the monolayer is oriented in a way that results in the submersion of a half of the V_{eff} in the subphase. C_{app} is therefore a sum of C_{inter} and $C_{sub}/2$. *B.* Positioning of the focus of the laser beam in the subphase allows the collection of signal coming only from the protein in solution. (Chwastek, 2013)

8. DISSOCIATION CONSTANT (K_D) DETERMINATION

To determine the dissociation constant, the lipid monolayer was titrated with protein by adding successively increasing protein concentrations to the subphase. As previously, protein was applied in 100 µL aliquots in SLB buffer and excess volume was removed after 1 min incubation. At each step, APD system was used to measure protein fluorescence intensity in the subphase and at the interface. The measurement was terminated once the saturation plateau was reached. Collected data were plotted versus initial protein concentration, knowing the concentration of used protein solution and assuming the subphase volume was constant over the duration of the experiment. Assuming protein fluorescence intensity proportional to protein concentration, fitting the Hill equation to a plot of protein intensity at the surface against total protein concentration allows determination of protein K_D (Shi et al, 2007). Applying it for monolayers, fluorescence intensity at the monolayer level (F) is a sigmoidal function of protein concentration (x) as described by equation 16, where F_{max} is the maximum fluorescence intensity at the interface and n is the Hill coefficient, which describes cooperativity of the interaction.

$$F(x) = F_{max} \frac{x^n}{K_D^n + x^n} \qquad \text{(eq. 16)}$$

III. RESULTS AND DISCUSSION

1. LIPID MIXTURE CHARACTERIZATION

* 1.1. Π-A ISOTHERMS

In order to study the influence of lipid packing on lipid-protein interactions, a lipid monolayer approach was chosen. Due to the risk of lipid oxidation by carbon-chain exposure to air after lipid deposition in the air-water interface, fully saturated DMPC was used as a representative glycerophospholipid. Even though the T_m (≈ 23 °C) (reviewed in Koynova & Caffrey, 1998) is very close to the room temperature (≈ 23.3 °C), it is predicted that the DMPC monolayer presents as homogeneous fluid phase – liquid extended (*LE*). Only at high surface pressures near the collapsing point of the monolayer, it should be possible to obtain a solid phase (*S*). The surface pressure (π)-area (A) isotherms obtained either on water or on buffer (fig. 1) go in agreement with those described in literature (Sabatini et al, 2008; Wilke et al, 2010). The isotherm compression is accompanied by an increase in surface pressure till monolayer collapses around 45 *MMA* (mean molecular area, in Å^2). The absence of a plateau or a sudden change in the isotherm points towards a homogeneous LE phase in the whole range of compression. Also, the used SLB buffer shows no apparent influence in the isotherm shape and lipid behavior.

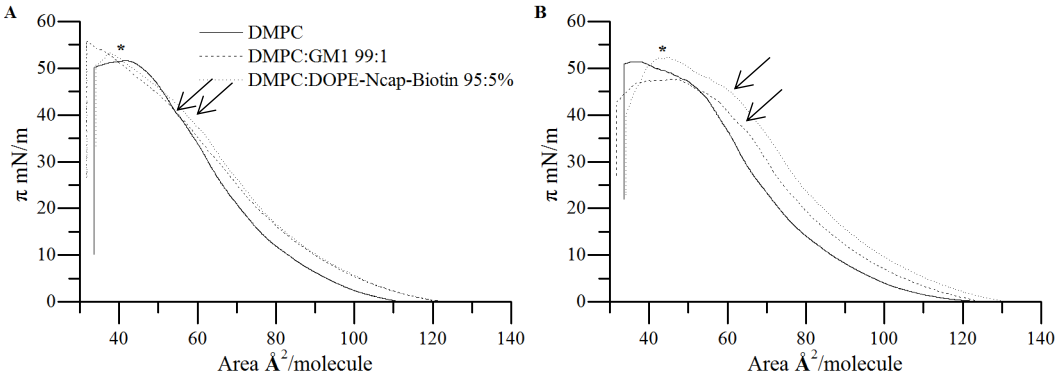

Fig. 1: Representative π-A isotherms of DMPC, DMPC:G_{M1} 99:1 and DMPC:DOPE-Ncap-Biotin 95:5 on water (*A*) and on SLB buffer (*B*) subphase. The arrows point possible phase transitions from LE to S for non-pure DMPC monolayers and the * corresponds to the collapsing region of the monolayers.

Besides the characterization of pure DMPC monolayer, mixtures containing small percentage of G_{M1} and DOPE-Ncap-Biotin were analyzed in order to study the effect of specific ligand on protein-monolayer interaction for choleratoxin and streptavidin, respectively. 5 mol % DOPE-Ncap-Biotin and 1 mol % G_{M1} were used in order to ensure monolayer homogeneity (Rock et al, 1991; Shi et al, 2007). The respective isotherms (fig. 1), both on water and on buffer, were slightly shifted to higher surface pressures. The effect of G_{M1}, even though in smaller molar percentage, was superior to that of DOPE-Ncap-Biotin, especially on buffer, most probably due to its large area/volume occupied by the head group of this lipid (65 Å^2 for G_{M1} compared to 42.5 Å^2 for DMPC). Even though, the critical area at which the collapse pressure is reached didn't suffer any change with the presence of both G_{M1} and DOPE-Ncap-Biotin, as it would be

expected from the small concentration in which they are present. Moreover, in accordance with published data for other lipid mixtures containing G_{M1} (Yuan & Johnston, 2000; Kycia et al, 2011), the shape of the isotherm was not heavily modified, indicating a monolayer in *LE* phase up to ≈ 60 *MMA*. Around this value, for both mixtures a small kink in the isotherm was observed which can be an evidence for a phase transition to the *S* state. Once again, the SLB buffer did not show any major impact on shape of isotherms.

* 1.2. STRUCTURAL CHARACTERIZATION

For further characterization, monolayers at different *MMA* were imaged using to miniaturized chambers coupled with confocal microscopy (Chwastek & Schwille, 2013). As a fluorescent dye, Chol 542 was added to DMPC, DMPC:G_{M1} 99:1 and DMPC:DOPE-Ncap-biotin 95:5 lipid mixtures at concentration which assure monolayer visualization and do not interfere with the monolayer organization. In accordance with previous studies, a Chol 542 concentration of 0.05 mol % was used with no influence on the monolayer isotherm, as observed in control measurements (not shown). Lipid monolayer imaging (fig. 2) revealed that in the range of analyzed *MMA* (50 to 100 $Å^2$), the three analyzed mixture have a mostly homogeneous deposition at the air-water interface. However both at low (100 *MMA*) and high (60 – 50 *MMA*) pressures the monolayer shows slight variations. At 100 *MMA,* some rapidly diffusing gas domains (*G*) are still formed due to the small amount of lipids deposited at the interface and low surface tension resulted from loose molecular packing. On the other hand, with the increase in surface pressure, dye clusters tend to form. Moreover, some small non-defined domains can be found at 50 *MMA*. The presence of fast-diffusing domains due to air flow, sample tilt and microscope/table vibration may hamper APD usage for further studies as the stability of the signal is compromised. Nonetheless, whether pure DMPC or its mixtures with G_{M1} or DOPE-Ncap-Biotin, monolayers have a general homogeneous appearance, irrespectively from the type of subphase. Thus this system fulfills requirements for being used in FCS studies.

* 1.3. DIFFUSION COEFFICIENT DETERMINATION

In order to confirm the stability and reproducibility of the system, FCS studies were performed on DMPC monolayers deposited at different π in a buffer-air interface, as previous studies showed a very small influence of SLB buffer on lipid diffusion (Chwastek & Schwille, 2013). To avoid APD saturation, a concentration of around 0.01 mol % Chol 542 was used. From the time correlation of the signal and its fitting to a 2D 2 component model (eq. 13), which accounts not only for the two dimensional diffusion of the dye, but also for the monolayer vibration and the fraction of particles that transit for the triplet state, lipid diffusion can be determined through equation 9. For that, a previous system calibration is needed – several dilutions of Alexa 546 (*D* = 341 $\mu m^2/s$ (Petrasek & Schwille, 2008)) were used to determine r_0^2 through correlation curve fitting to a 3D model (eq. 12).

Previous studies have shown that an increased lipid density slows lipid mobility (Gudmand et al, 2009). This is also observed in the current system (Chwastek & Schwille, 2013), shifting the correlation curves towards slower diffusion times (fig. 3.*A*). Analyzing the corresponding diffusion coefficients as a function of *MMA*, a linear tendency is obtained as expected from the

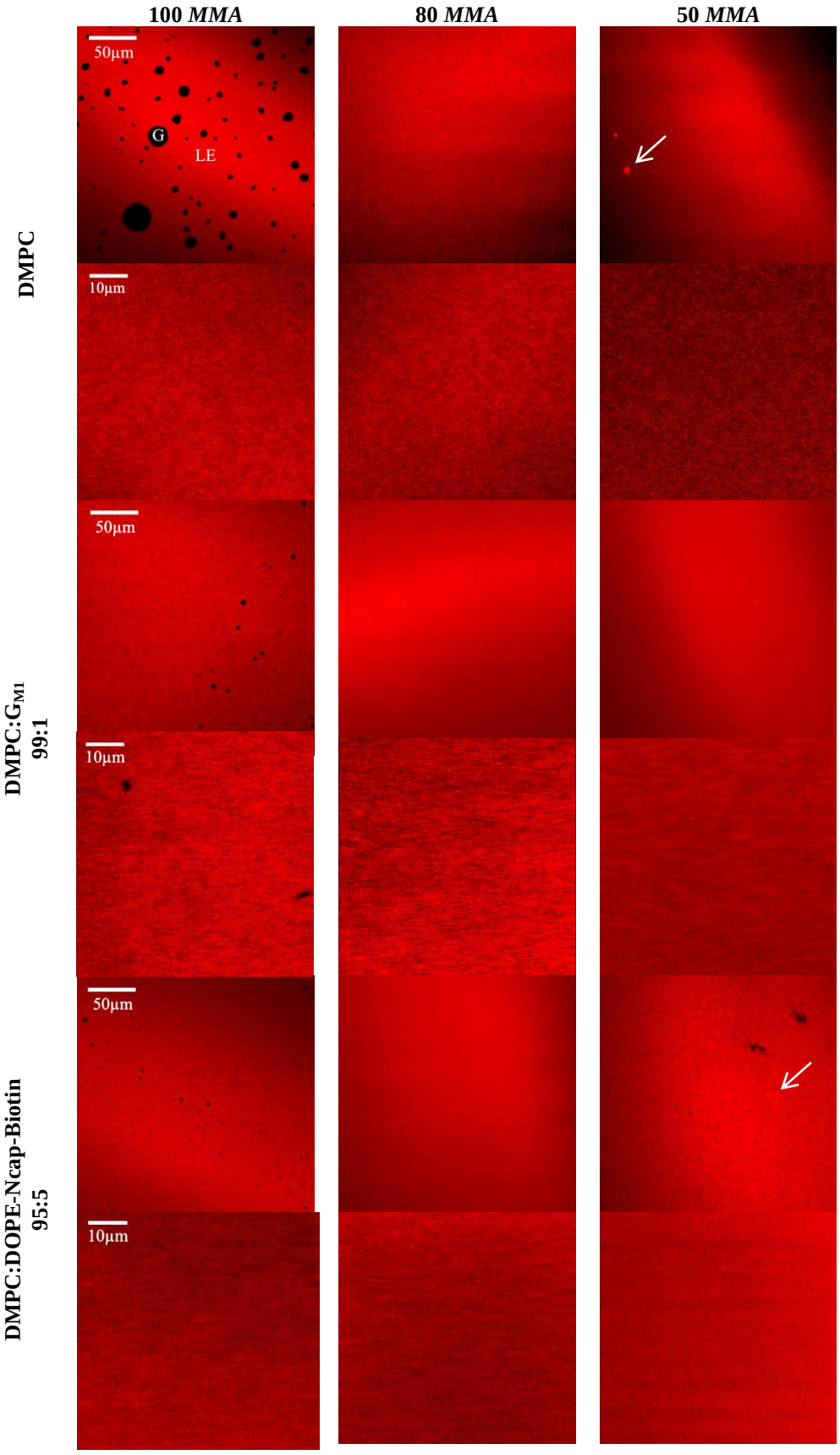

Fig. 2: Representative confocal microscopy images of different DMPC monolayers (pure, 1 mol % GM1 and 5 mol % DOPE-Ncap-Biotin) at 100, 80 and 50 *MMA*, labeled with 0.05 mol % Chol 542. Scale bars are presented in the first image of each row. Representative lipid phases are denoted at DMPC 100 *MMA*. White arrows point towards dye clusters.

free area model (FAM) (Galla et al, 1979) and previously experimentally proved (Gudmand et al, 2009; Chwastek & Schwille, 2013) (fig. 3.*B*). The intersection of the obtained linear fit with the horizontal axis corresponds to the theoretical *MMA* at which the lipid diffusion coefficient equals zero – critical point (*ac*). In the above experiment, *ac* was 36.0 ± 4.7 Å^2/molecule which deviates slightly from previously reported values for the same lipid (42.5 ± 7.5 Å^2 (Chwastek & Schwille, 2013) / ≈ 47 Å^2 (Gudmand et al, 2009)) most probably due to the error associated with the extreme points of the fit – 100 *MMA* when the presence of small gas phases can influence the measurements and at 50 *MMA* when the high pressure and formation of *S* phase may influence lipid deposition. Moreover, control experiments showed that the presence of G_{M1} or DOPE-Ncap-Biotin in the monolayer did not alter significantly lipid mobility (not shown).

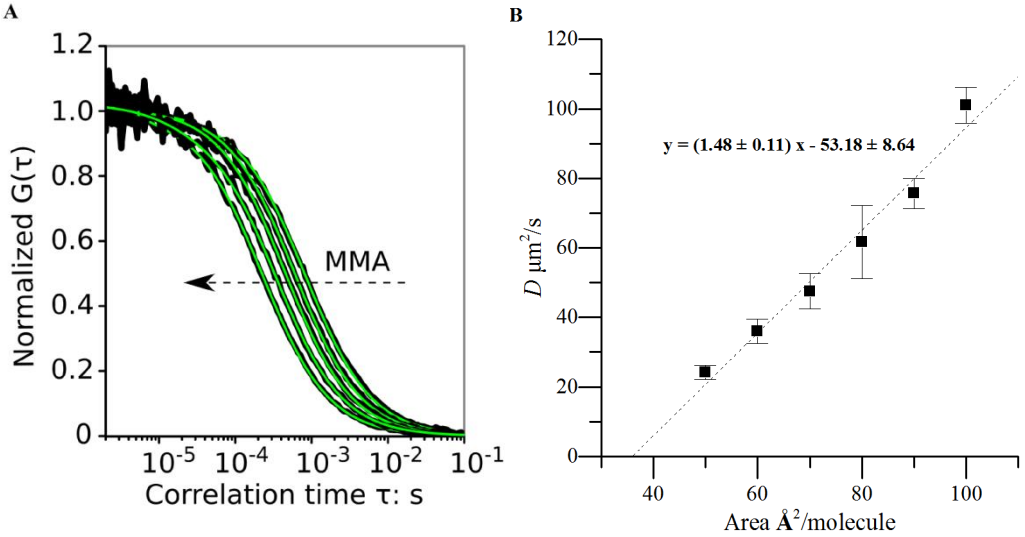

Fig. 3: *A.* Average correlation curves (black) of Chol 542 in DMPC monolayers deposited on a SLB buffer subphase. Green lines represent fits to eq. 13. The arrow indicates increasing *MMA* – 50, 60, 70, 80 and 90 Å^2 approximately. From (Chwastek & Schwille, 2013) *B.* Diffusion coefficients as a function of *MMA* and corresponding linear fit (dashed line).

* 1.4. DYE DISTRIBUTION

With the increase of lipid density at lower *MMA,* it is expected that the number of particles *N* in the focal volume V_{eff} increases. Nonetheless, that was not observed in the performed experiments (fig. 4) – not only the distribution of the lipid dye was not increasing proportionally to π, but also the fluorophore showed a non-homogeneous distribution within the monolayer.

In order to address the problem of abnormal dye distribution it was first investigated whether the effect is was due to the dye sterol nature the Chol 542 label was substituted by an equivalent concentration of DiO – a lipophilic carbocyanine. On the other hand, given the DMPC T_m temperature in the range of the room temperature and the possibility of small temperature gradients within the monolayer caused by the laser heating, *N* variation with *MMA* in monolayers formed of phospholipids with lower T_m was also studied. Therefore pure DOPC, an unsaturated phospholipid with T_m = – 18 °C (reviewed in Koynova & Caffrey, 1998), labeled with 0.01 mol % Chol 542 was used in order to eliminate the influence of temperature.

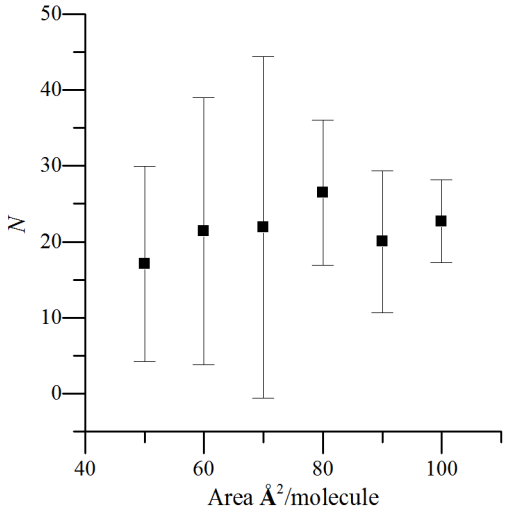

Fig. 4: Variation of number of particles of Chol 542 *N* in a DMPC monolayer deposited at different lipid densities on a SLB buffer subphase. Values obtained through fitting of eq. 13 to the corresponding correlation curves.

In both mixtures – DMPC 0.01 mol % DiO and DOPC 0.01 mol % Chol 542 – diffusion coefficient shows the same trend previously verified for DMPC 0.01 mol % Chol 542 – with increasing lipid density the lipid mobility decreases linearly (fig.5.*A*-*B*). The critical point is 37.2 ± 13.5 Å^2/molecule for DMPC (in agreement with the previous results) and 32.7 ± 12.7 Å^2/molecule for DOPC. Having in mind its molecular area (72.2 Å^2 obtained in SLBs at 30 ^{o}C (Tristram-Nagle et al, 1998)), the obtained *ac* value for DOPC is deviated from the expected, most probably due to errors at the extremes of lipid density in study (70 and 120 *MMA*). Note that the experiments presented here were performed at a lower temperature (23 ^{o}C) which should contribute for a lower *ac* as the thermal motion of the free rotating bonds is reduced. Nevertheless, the diffusion coefficient variation with lipid packing seems to be in good agreement with the predicted by FAM. Nevertheless, as for DMPC labeled with Chol 542, the number of fluorophore particles in the monolayer does not vary linearly with increased lipid density. So, neither fluorescent probe nor phospholipid nature seems to influence the detected number of particles. The study of probe partition in different lipid monolayers at increasing surface pressures could probably give a hint about the reason for its abnormal distribution within the monolayer.

Nevertheless, the system appears to be quite reproducible regarding lipid monolayer deposition, packing and mobility. Thus, it is possible to proceed to further studies, namely protein binding assays.

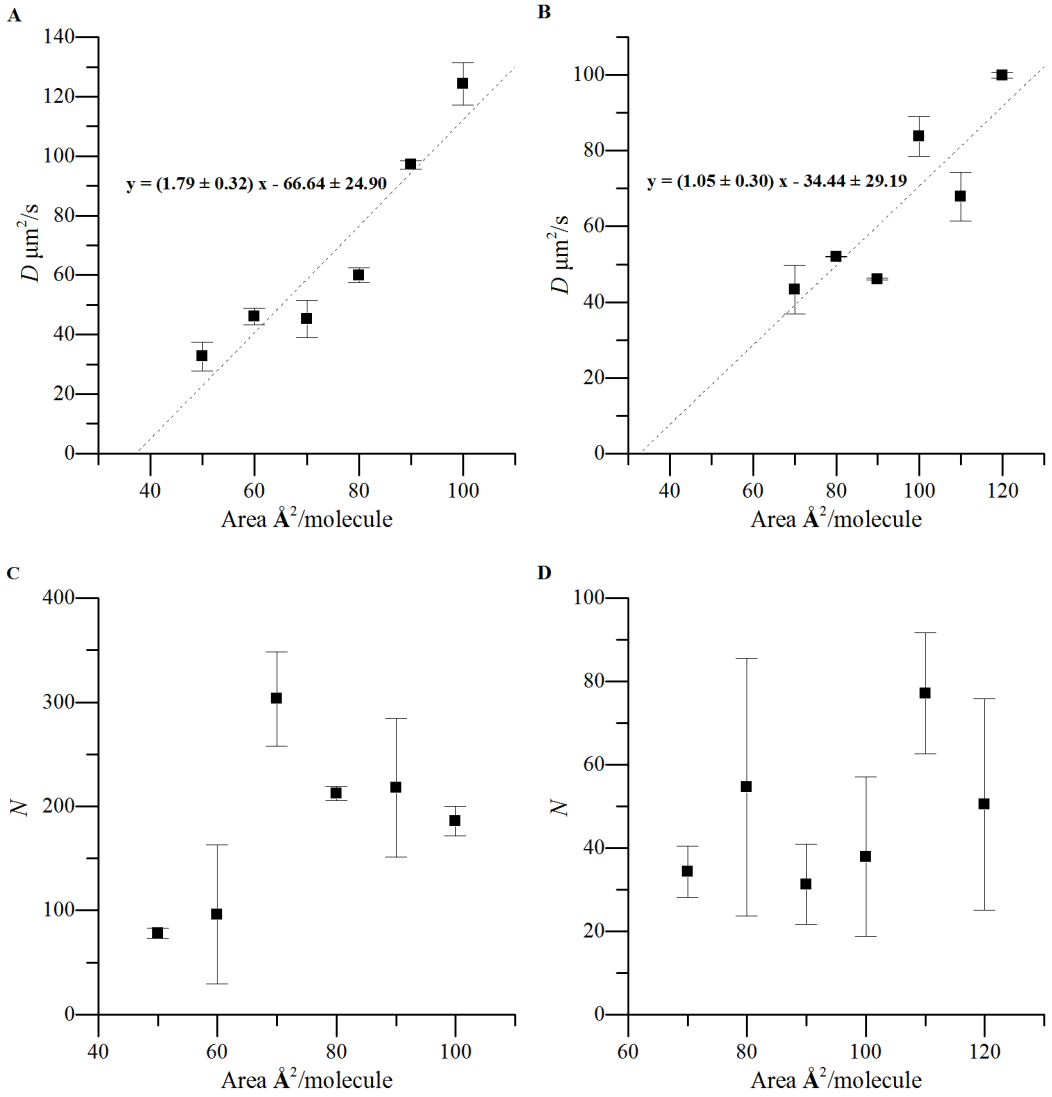

Fig. 5: Diffusion coefficients *D* as a function of *MMA* and corresponding linear fit (dashed line) of (*A*) DMPC labeled with 0.01 mol % DiO and of (*B*) DOPC labeled with 0.01 mol % Chol 542. Number of particles *N* obtained from the fitting of eq. 13 to the correlation curves – correspondingly *C* and *D*.

2. STREPTAVIDIN BINDING TO LIPID MONOLAYER

* 2.1. INFLUENCE OF LIPID PACKING IN HOMOGENEOUS MONOLAYERS

In order to study protein-monolayer interaction, an APD system was used to measure streptavidin-Alexa488 fluorescence intensity at the SLB buffer subphase and at the interface (fig. 6). DMPC lipid monolayers were deposited at the buffer-air interface with different lipid densities. After confirming the integrity of the monolayer (as described in Results and discussion; 1.1. to 1.3.), 100 µL protein solution was added to the subphase in order to reach an initial concentration of 100 nM, as it is expected that streptavidin doesn't bind strongly to the lipid interface. Each sample was measured after 1 min incubation and removal of excess volume.

Fluorescence intensity of streptavidin is much higher at the monolayer interface than in the subphase, which is in accordance with the difference in count rate per molecule of Alexa 488

in presence and absence of lipids, as described in literature for a variety of fluorescent probes (reviewed in Valeur, 2002; Lakowicz, 2006). Due to the difference in polarity of surrounding medium, the non-radiative processes are increased in the buffer subphase which contributes to the reduction of the probe's quantum yield. Moreover, at a constant protein concentration, the fluorescence intensity at the interface increases with increasing *MMA,* while it remains constant in the subphase (excluding 50 *MMA*) which points towards the dependence of protein binding on lipid packing. A quantification of the ratio between the interface and subphase fluorescence intensities indicates that streptavidin binding to DMPC monolayer might be dependent on lipid packing (fig. 7.*A*) and therefore also on the lipid diffusion (fig. 7.*B*), being higher at a loose packing. Interestingly, this tendency had already been proposed four decades ago based on surface pressure variation studies induced by protein addition to PC monolayers at different physical states (Phillips et al, 1975) and glycosphingolipid

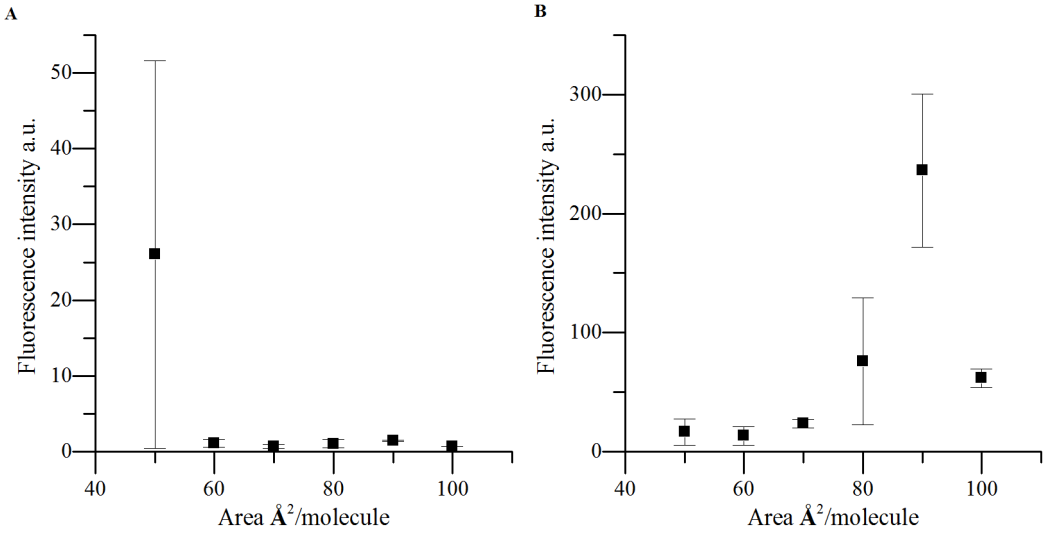

Fig. 6: Fluorescence intensity of streptavidin-Alexa 488 (100 nM) in the subphase (*A*) and interface (*B*) of a DMPC monolayer system deposited at the SLB buffer-air interface.

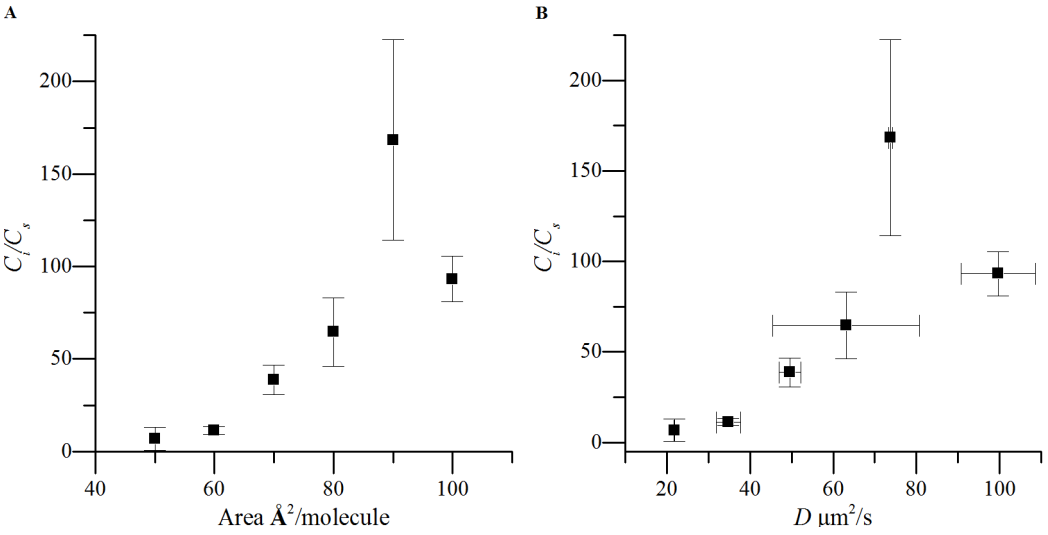

Fig. 7: Streptavidin-Alexa 488 (100 nM) binding (C_i/C_s) to DMPC monolayers as a function of *MMA* (*A*) and *D* (*B*).

monolayers at different π (Fidelio et al, 1981). However, at lower lipid density (100 *MMA*), where the lipids are loosely packed and formation of G phases is possible (fig. 2), streptavidin binding reduces again. Moreover, in a pure buffer-air interface streptavidin binding is relatively low (C_i/C_s = 14.0 ± 8.1), which suggests that the protein is not surface active and requires lipid for proper binding to the interface. Thus the data suggest that streptavidin establishes weak interactions with lipid molecules but further studies are needed to characterize the precise nature (hydrophobic or electrostatic) of the this interaction. This can be analyzed by varying the buffer conditions (pH, ion concentration and composition) as well as the chain length and saturation of monolayer phospholipids.

* 2.2. Influence of phase separation

In order to illustrate the dependence of the protein-monolayer interaction on lipid packing, protein behavior in presence of different phase separated lipid monolayers was studied. The reason for this is that the liquid condensed (LC)/ S phase lipid molecules are more tightly packed then in the LE phase. After obtaining the π-A isotherms of DMPC:DSPC 1:1, DPPC, DOPC:bSM:Chol 1:1:1 and DPPC:Chol 7:3 lipid mixtures (fig. 8), lipid monolayers were deposited at a similar surface pressure (7-12 mN/m) in order to obtain phase separation. This surface pressure is in the range of the isotherm plateau observed for pure DPPC – at this constant π, phase coexistence is possible by gradual transition of lipid molecules from LE to LC solid-like phase, resulting in a decrease in *MMA* (Phillips & Chapman, 1968). In the other mixtures, no plateau is observed as the lipids organize spontaneously in two phases (LE and LC in case of DOPC:bSM:Chol 1:1:1 and DPPC:Chol 7:3; LE and S in case of DMPC:DSPC 1:1) due to their physico-chemical nature (Kim et al, 2001; Yun et al, 2003; Sabatini et al, 2008; Wilke et al, 2010). All mixtures were labeled with 0.05 mol % Chol 542 – previous studies had shown that in monolayers, as in bilayers, the probe preferentially partitions into the LE phase in comparison to S or LC (corresponding to ld, gel and lo phases respectively in bilayers) (Chwastek & Schwille, 2013). An initial concentration of around 50-100 nM streptavidin was added and samples were imaged through confocal microscopy (fig. 9).

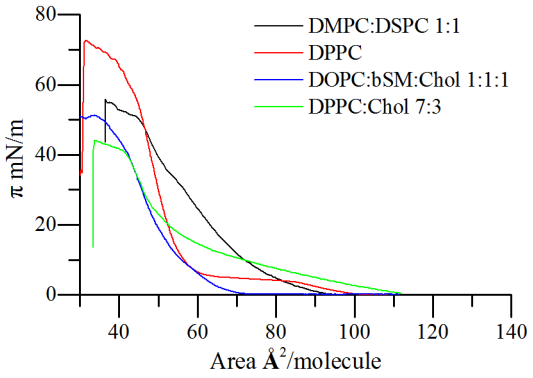

Fig. 8: π-A isotherm of DMPC:DSPC 1:1, DPPC, DOPC:bDM:Chol 1:1:1 and DPPC:Chol 7:3 lipid mixtures.

All monolayers showed a phase separation, with dark S/LC domains in a bright homogeneous LE background (fig. 9). The poor contrast in case of DMPC:DSPC 1:1 is probably due to the high S phase content of the sample even though it was expected to occupy 25 % of the area (Wilke

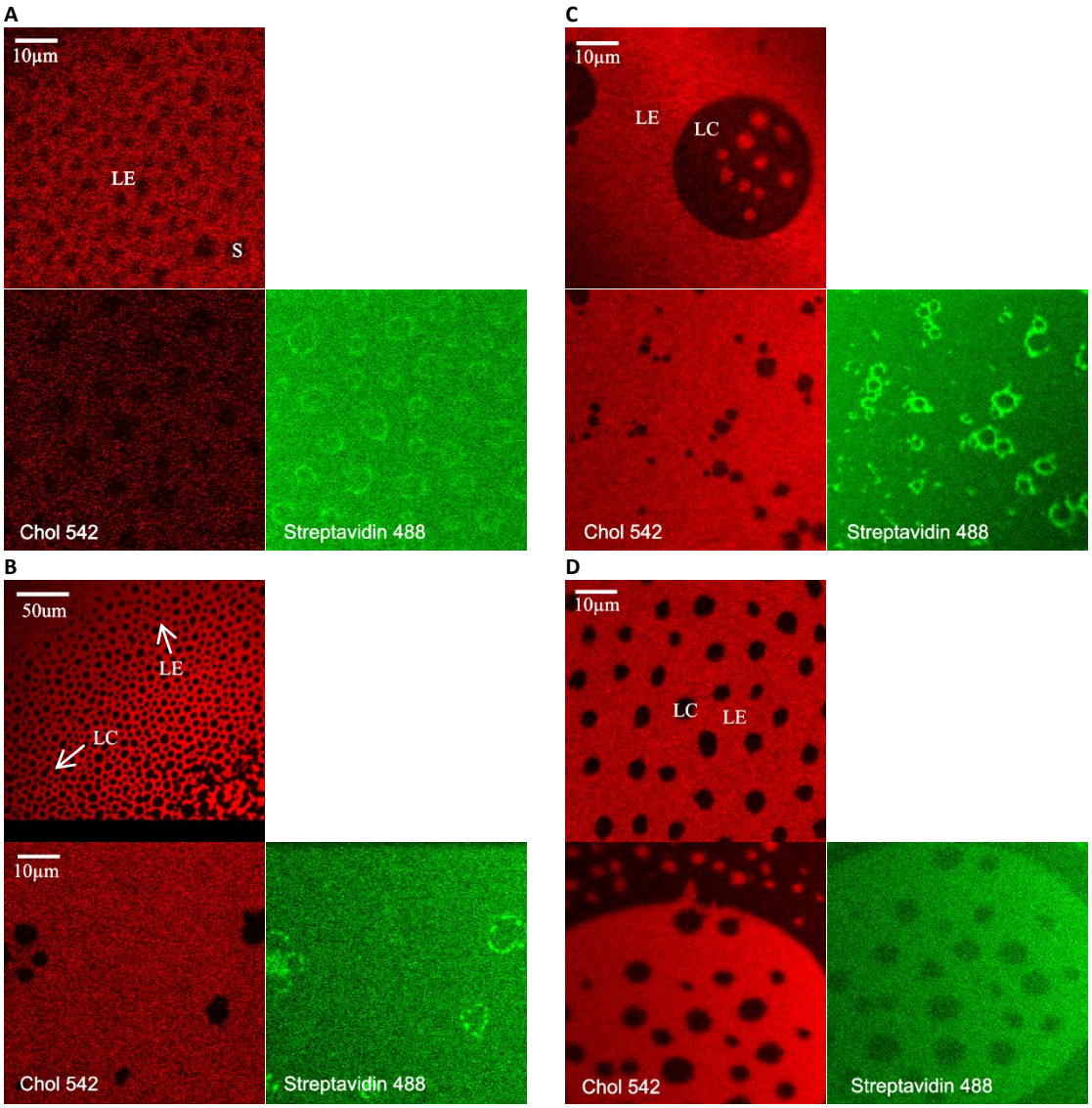

Fig. 9: Representative images of streptavidin-Alexa 488 (50-100nM) binding to DMPC:DSPC 1:1 (*A*), DPPC (*B*), DOPC:bSM:Chol 1:1:1 (*C*) and DPPC:Chol 7:3 (*D*) phase separated monolayers labeled with Chol 542 0.05 mol %. Images of the lipid monolayer before protein addition are also shown – representative phases are marked.

et al, 2010). According to the observed dependence of protein binding on lipid packing (fig. 7), a higher protein fluorescence intensity was expected in LE phase in comparison to the LC/S phase in phase separated mixtures. In contrast, in DMPC:DSPC 1:1, DPPC and DOPC:bSM:Chol 1:1:1 monolayers streptavidin tends to accumulate at domain boarders, the interface of the fluid and solid phases. Moreover, no significant difference in fluorescence intensity of protein was observed between the phases. Only DPPC:Chol 7:3 monolayer streptavidin shows a behavior coherent with the binding curves (fig. 7) – there is a preference in binding to the LE phase compared to LC phase. This results might be explained by the difference in lipid packing between LC/S and LE phase – in DMPC:DSPC 1:1 the phase separation is extreme, between a highly packed S phase and a fluid LE phase; pure DPPC phase separates in LE and LC gel-like phases; DOPC:bSM:Chol 1:1:1 and DPPC:Chol 1:1 are both raft-like phase separations. Nonetheless, DPPC:Chol 1:1 presents a lower difference in lipid packing between phases when compared to DOPC:bSM:Chol 1:1:1, according to previous studies in phase separated GUVs

labeled with Laurdan dyes (Bagatolli & Gratton, 2000; Sezgin unpublished results on giant plasma membrane vesicles). Moreover, other molecules – such as fatty acids and various peptides – tend to accumulate in the grain boundaries of domains with high lipid order (line defects with increased hydration) or are distributed in the interface of phases with high lipid packing difference (Nuscher et al, 2004; Franquelim et al, 2010; Yarrow & Kuipers, 2011; Khmelinskaia et al, 2013). Thus, it is not surprising to see a similar effect in streptavidin binding to phase separated monolayers. In summary, the results imply an important role of phase separation in controlling protein binding and its sorting at the membrane.

* 2.3. INFLUENCE OF THE PRESENCE OF A BIOTINYLATED LIPID

Proceeding further, the studies aimed at exploiting the strong binding of streptavidin to biotin by incorporating a biotinylated lipid – DOPE-Ncap-Biotin – into the monolayer. Thus, binding curve of streptavidin to DMPC:DOPE-Ncap-Biotin 95:5 monolayers were obtained (fig. 10).

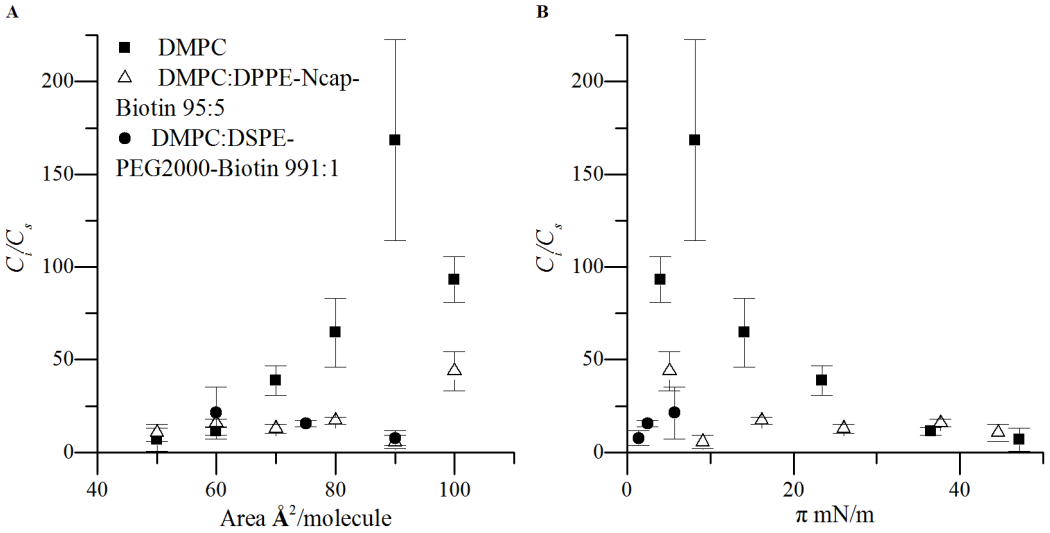

Fig. 10: Streptavidin-Alexa 488 (100 nM) binding (C_i/C_s) to DMPC, DMPC:DPPE-Ncap-Biotin 95:5, DMPC:DSPE-PEG2000-Biotin 99:1 monolayers as a function of *MMA* (*A*) and pressure (*B*). Pressure values are averaged from the respective π-A isotherms (fig. 1 and 13).

Interestingly, the presence of DPPE-Ncap-Biotin instead of increasing streptavidin concentration at the interface, reduced this interaction. Although this biotinylated lipid is widely used for specific binding assays, usually an altered form of streptavidin/avidin is used that abolishes unspecific binding (e.g. Sarmento et al, 2012; Vogel & Schwille, 2012; Heinemann et al, 2013). Additional evidences of strongly suppressed streptavidin binding to DPPE-Ncap-Biotin due to steric hindrance or inaccessibility of biotin for the binding spot from the actin-myosin minimal system (Vogel & Schwille, 2012), might partially explain the obtained result. Note that for biotin binding to neighboring subunits in streptavidin, a fixed distance of 20 Å should be retained as otherwise the binding will be sterically hindered (Hendrickson et al, 1989). It is also possible that the addition of DPPE-Ncap-biotin to the monolayer increases the surface pressure in a way that prevents streptavidin binding. Nevertheless, π-A isotherm (fig. 1) previously showed that the increase in surface pressure is not significant and thus this possibility is overruled (fig. 10.*B*).

In Vogel and Schwille 2012, this problem was overcome by using DSPE-PEG2000-Biotin. Thus this molecule appeared as a valid alternative for a specific membrane ligand for streptavidin. However, the protein binding curve obtained for DMPC:DSPE-PEG2000-Biotin 99:1 monolayer at different lipid densities showed the same trend observed with DPPE-Ncap-Biotin – streptavidin binds very poorly to the monolayer at all analyzed lipid densities and even lower than in absence of a biotinylated lipid (fig. 10). One possible reason could be the inaccessibility of biotin to streptavidin binding due to PEG2000 tail conformation in the monolayer. Moreover, in lipid monolayers long-chained PEG molecules present three conformations (fig. 11) – at high *MMA* PEG molecules assume a pancake conformation in which the PEG tails are extended along the water-air interface; when the lipid density increases, PEG tails assume globular mushroom conformation; at high surface pressures, PEG chains extend towards the subphase in a brush conformation (Baekmark et al, 1995).

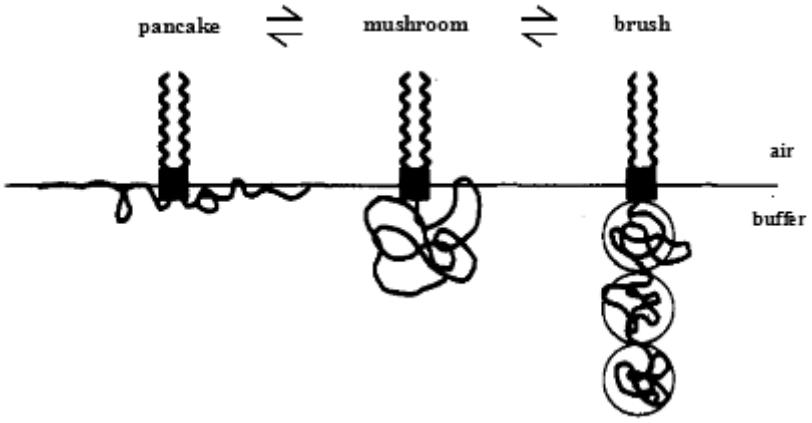

Fig. 11: Schematic representation of the three possible conformations for long-chained PEG-ylated lipid – pancakes (*A*), mushroom (*B*) and brush (*C*) conformation. Adapted from (Baekmark et al, 1995).

Moreover, in the mushroom conformation, DSPE-PEG2000 has a molecular area two orders of magnitude higher (3719 $Å^2$ (Allen et al, 2002)) than that of regular phospholipids (40-70 $Å^2$). Thus, surface coverage by PEG chains plays an important role in protein interactions with lipid layers (Kim et al, 2000; Auguste et al, 2008).

Taking into account the head area of DSPE-PEG2000 and the number of molecules of PEGylated lipids present in the monolayer at different lipid densities, it was possible to calculate the surface coverage by PEG tails in mixtures containing different concentrations of DSPE-PEG2000-Biotin (fig. 12), as done for other systems (Allen et al, 2002). At low DSPE-PEG2000 concentrations (0.1 mol %), the surface coverage is almost independent of the lipid density and it never excesses 10 %. When the concentration increases to 1 mol % the surface coverage increases strongly with *MMA* decrease from 40 to 80 %. At 5 mol %, PEG side chains completely cover the surface at all *MMA*.

Furthermore, literature suggests that due to the high molecular area and the possibility of three chain conformations, the presence of long-chain PEGylated lipids will modify monolayer properties (Tanwir & Tsoukanova, 2008; Tsoukanova & Salesse, 2008). Thus, the obtained π-A isotherm for DMPC:DSPE-PEG2000-Biotin (fig. 13) not only is strongly shifted towards higher *MMA* in comparison to pure DMPC but also presents two main discontinuities – a pseudo

plateau around 11 mN/m corresponding to the mushroom to pancake transition and a second one due to DMPC transition from LE to S and consequent monolayer collapse, as described for other lipid mixtures containing the DSPE-PEG2000 (Tanwir & Tsoukanova, 2008).

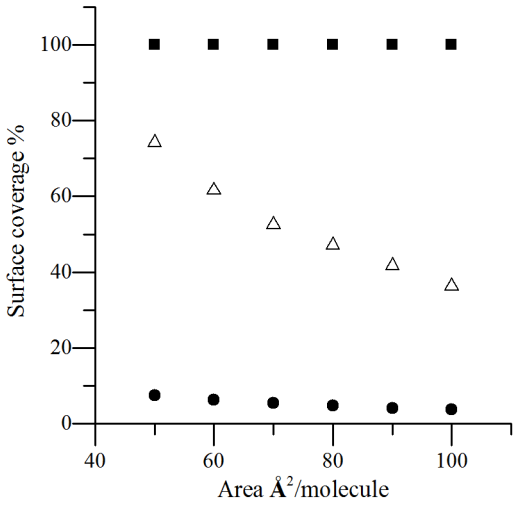

Fig. 12: Surface coverage (%) by PEG chains in DMPC mixtures containing 0.1 (•), 1 (Δ) and 5 mol % (■) DSPE-PEG2000-Biotin.

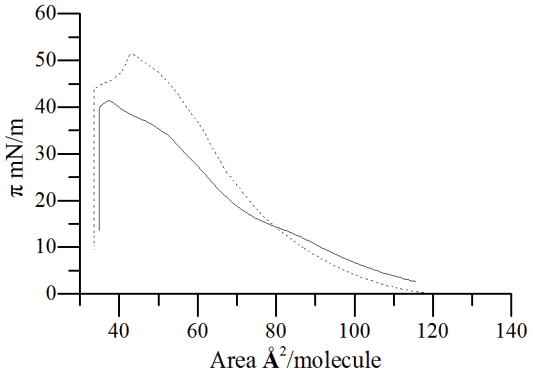

Fig. 13: π-A isotherm of DMPC:DSPE-PEG2000-Biotin 99:1 lipid mixtures. Pure DMPC isotherm is also represented for a better comparison – dashed line.

Moreover, monolayer imaging revealed the presence of undefined dark PEG-rich domains in the entire range of *MMA* studied, in accordance to previous studies (Tanwir & Tsoukanova, 2008), even at concentrations as low as 0.2 mol % DSPE-PEG2000-Biotin and at low lipid densities (fig. 14). Additionally, lipid dye appears to cluster in presence of larger domains, contributing to a non-homogeneous signal. Thus, the conformational transitions of the long PEG chains might explain the shielding of streptavidin binding to DMPC monolayers containing DSPE-PEG2000-Biotin (fig. 10).

Since in literature, the conformational transitions and domain formation and their effect on model membranes are mainly described for PEG molecules with long chains (Rex et al, 1998; Georgiev et al, 2007; Tsoukanova & Salesse, 2008; Stepniewski et al, 2011), DMPC mixture containing 0.1 mol % DOPE-PEG350 was morphologically characterized by confocal microscopy (fig. 15).

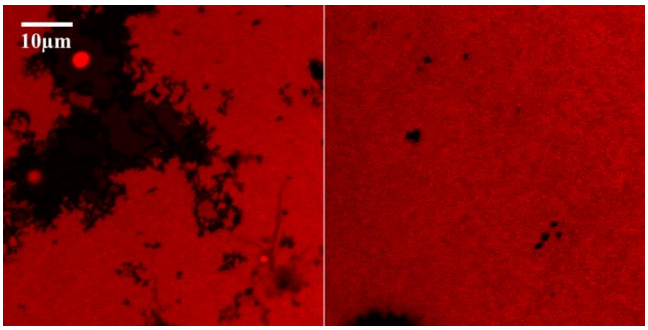

Fig. 14: Representative images of DMPC monolayers (100 *MMA*) containing 0.2 mol % DSPE-PEG2000-Biotin. The black domains correspond to PEG-rich domains.

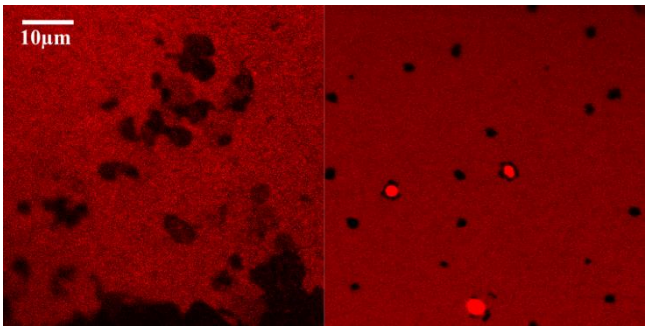

Fig. 15: Representative images of DMPC monolayers (100 *MMA*) containing 0.1 mol % DOPE-PEG350. The black domains correspond to PEG-rich domains.

Despite the much shorter PEG chains and lower molecular area (468 $Å^2$/molecule for DSPE-PEG350 (Allen et al, 2002)) of the functionalized lipids and thus a lower surface coverage, the DMPC monolayers didn't present a homogeneous morphology – several irregular domains were observed, which point towards a similar behavior to that observed with DSPE-PEG2000-Biotin.

A further possibility to obtain the specific streptavidin – biotin binding would be substituting native streptavidin for ExtrAvidin or NeutrAvidin – mutant (strept)avidin forms which retain the high protein stability and binding avidity but reduces the unspecific binding. Both protein forms were successfully used in assays involving correspondingly DPPE-Ncap-Biotin and DSPE-PEG2000-Biotin incorporation in lipid bilayers (Sarmento et al, 2012; Vogel & Schwille, 2012; Heinemann et al, 2013).

3. CHOLERA TOXIN *B* BINDING TO LIPID MONOLAYER

* 3.1. INFLUENCE OF LIPID PACKING ON $CTXB_5$ BINDING TO MONOLAYERS WITH DIFFERENT G_{M1} CONTENT

Besides streptavidin, Ctx binding to lipid monolayers was studied as this protein has a natural ligand – the ganglioside G_{M1} – that incorporates in lipid layers. Due to its lack of toxicity and retained G_{M1} binding activity, the pentameric $CtxB_5$ ring was used. Fluorescence intensity measurements of $CtxB_5$-Alexa 488 in the subphase and at interface was used to assess the influence of not only lipid packing, but also G_{M1} and protein concentrations on $CtxB_5$ binding to the monolayer. The *MMA* was varied under three conditions (fig. 16): pure DMPC monolayer

incubated with 100 nM and also 5 nM protein and DMPC monolayer containing 0.1 mol % G_{M1} incubated with 5 nM protein. The G_{M1} content was reduced from 1 mol % (fig.1) to 0.1 mol % in order to avoid any possible influence on the monolayer morphology, taking into account the experience previously had with lipid mixtures containing a biotinylated lipid. Control π-A isotherm (not shown) didn't show any major alterations in comparison to pure DMPC, as previously shown for the mixture containing higher G_{M1} concentration (fig. 1).

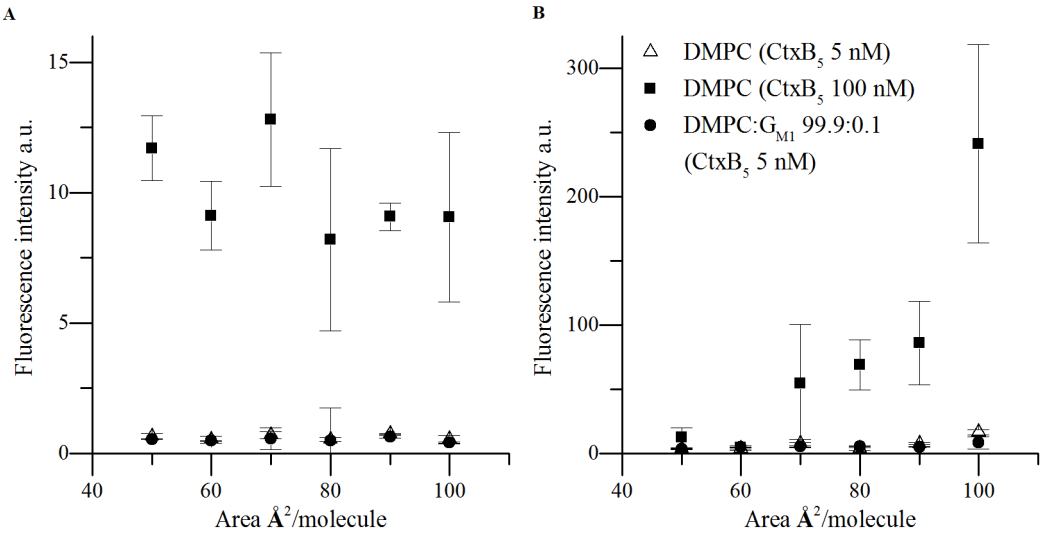

Fig. 16: Fluorescence intensity of Cholera toxin β-Alexa 488 in the subphase (*A*) and interface (*B*) of DMPC monolayer system with different G_{M1} content deposited at the SLB buffer-air interface – pure DMPC incubated with 5 nM and 100 nM $CtxB_5$; DMPC containing 0.1 mol % G_{M1} incubated with 5nM $CtxB_5$.

As previously observed for streptavidin (fig. 6), $CtxB_5$ fluorescence intensity at the monolayer interface is dependent on the lipid packing, especially at the high protein concentration (100 nM), while in the subphase it remains mainly constant, pointing towards a plausible dependence of protein binding on monolayer *MMA*. Also, the intensity of the protein at the monolayer level is generally higher than in the subphase, as expected from the change in Alexa 488 quantum yield according to polarity of surrounding medium. However, the difference in $CtxB_5$ intensities between subphase and interface appears to be much lower than the one observed for streptavidin at the same concentration (note the higher fluorescence intensity in the subphase of $CtxB_5$ (≈ 10 a.u.) compared to that of streptavidin (≈ 1 a.u.) – fig. 16.*A* and 6.*A* respectively). This implies a lower membrane binding of Ctx compared to streptavidin. As fluorescence intensity is proportional to fluorophore concentration (eq. 14), an increase of fluorescence intensity in both subphase and monolayer interface at higher protein concentrations is observed. For further analysis, protein binding was quantified through ratio of interface and subphase intensities (see Materials and Methods; 7) (fig. 17).

The previously observed streptavidin binding dependence on monolayer lipid packing (fig. 7.*A*) is manifested only at high protein concentrations in case of $CtxB_5$. At a starting protein concentration of 100 nM, $CtxB_5$ binding increases with lipid *MMA* in pure DMPC monolayers, suggesting that protein binding is dependent on surface pressure which is in accordance with previous studies (Fidelio et al, 1981). On the other hand, at a concentration as low as 5 nM, protein concentration appears to be rather independent of lipid packing. Thus, the

concentration of protein reservoir influences $CtxB_5$ binding to lipid monolayer, as had been proposed four decades ago in Ctx, melittin and myelin penetration in ganglioside monolayers (Fidelio et al, 1981; Cumar et al, 1982). Further, when comparing streptavidin binding to pure buffer-air interface (C_i/C_s = 14.0 ± 8.1) to that of $CtxB_5$ (C_i/C_s = 150.8 ± 32.8) at the same initial protein concentration (100 nM), the latter protein reveals rather higher surface activity. Nevertheless, the overall binding of streptavidin to the monolayer (C_i/C_s > 10 – fig. 7) is higher than that one of $CtxB_5$ (C_i/C_s < = 10 – fig. 17). This distinct protein behavior must be related to protein structure as the interaction with the interface emerges from the establishment of several weak interactions of its components with protein amino-acid residues. So, additional binding assays in different buffer conditions are needed in order to understand the nature of the protein-monolayer interaction.

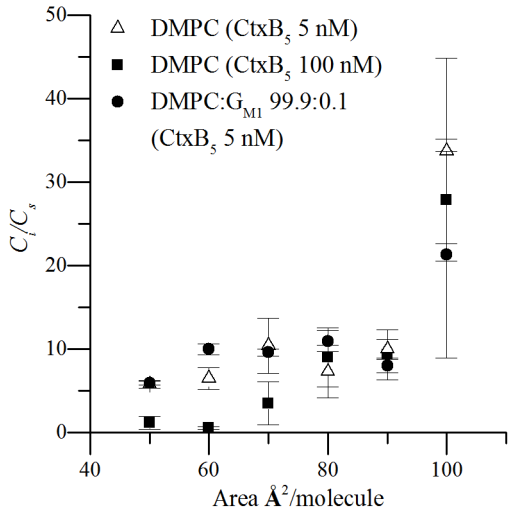

Fig. 17: $CtxB_5$-Alexa 488 binding (C_i/C_s) to DMPC monolayers with different G_{M1} content as a function of *MMA* – pure DMPC incubated with 5 nM and 100 nM $CtxB_5$; DMPC containing 0.1 mol % G_{M1} incubated with 5nM $CtxB_5$.

When analyzing the influence of G_{M1} presence in the monolayer, an increase of $CtxB_5$ binding to the monolayer is expected due to the specificity of the ligand-protein binding. Accordingly, a slight increase of $CtxB_5$ binding is observed when a small concentration (0.1 mol %) of ganglioside is incorporated. Interestingly, the observed trend relative to lipid density at low protein concentration is the same in absence or presence of G_{M1} – the protein binding is mainly constant through the studied lipid densities. This suggests that even at high pressures G_{M1} is homogeneously distributed in the monolayer in a way which allows $CtxB_5$ binding. Nevertheless, at 50 *MMA* $CtxB_5$ binding to monolayer is not influenced by G_{M1} presence, probably due to increased ganglioside density that hinders protein-ligand interaction (Shi et al, 2007).

At 100 *MMA*, both protein and G_{M1} concentration effects are canceled – note the big error bars associated with the measurements. This might be explained by the possible formation of gas phases and variation of protein binding to zones of different lipid packing due to meniscus formed by subphase deposition or sample tilting. The increase in surface pressure associated with lipid deposition at the interface reduces the meniscus angle, thus reducing the variation in lipid density.

* 3.2. QUANTITATIVE ANALYSIS OF PROTEIN BINDING

For a better comparison of the influences of lipid packing and G_{M1} content on $CtxB_5$ binding to DMPC monolayers, lipid monolayer was titrated with increasing $CtxB_5$ concentration in order to obtain K_D values by fitting the Hill equation to the titration curve (eq. 16). At each concentration, protein fluorescence intensity was measured through APD system in the subphase and at the monolayer level. Four different conditions were studied: pure DMPC and 0.1 mol % G_{M1} containing DMPC monolayers, both at 50 and 90 *MMA*. Since the Alexa 488 signal was observed to have a high reflection component, due to the imperfect cut-off of the excitation wavelength by the available filter system, $CtxB_5$-Alexa 647 was used as the wavelength cut-off is much better aligned allowing a more accurate data acquisition.

The subphase $CtxB_5$ concentrations shows mostly linear dependency with increasing initial concentration at all conditions, not presenting major dependence either on G_{M1} content or lipid density (fig. 18.*A*). On the other hand, at the interface $CtxB_5$ appears to have a tendency to saturate the monolayer as at high protein concentration (above 70 nM) it becomes difficult to increase the membrane binding (fig. 18.*B*). A similar saturation was described on ganglioside monolayers and G_{M1} containing POPC (1-palmitoyl-2-oleoyl-*sn*-glycero-3-phosphocholine) SLBs (Cumar et al, 1982; Shi et al, 2007). Nonetheless, the values at which the protein saturates the surface are widely spread, not only due to difference in method accuracy but also in the protein pool available to bind the surface – note that the ratio of surface area and reservoir volume does influence the protein binding, as the same total amount of protein when available for a bigger area will appear as lower concentration of the protein on the membrane. At low protein concentrations, no difference between conditions is observed, as it is predicted from the $CtxB_5$ binding curve (fig. 17). However, with increasing protein concentration the fluorescence intensity at 90 MMA reaches higher values than at 50 MMA, suggesting a preferential $CtxB_5$ binding to less packed monolayers. Additionally, these results uncover the influence of G_{M1} on $CtxB_5$ binding to lipid monolayers that were not clear in the previous binding curve (fig. 17) – in presence of 0.1 mol % of ganglioside, the fluorescence intensity increases globally as the amount of protein binding to the monolayer increases. Also, subphase concentration is in general never higher than that of the interface, in accordance with the higher fluorophore quantum yield when inserted in a non-polar environment. It's predicted that this behavior is overcome once the saturation plateau is established and the protein accumulates in the subphase reaching much higher concentrations – note that at high protein concentration (90-130 *MMA*) in absence of $G_{M1,}$ the protein fluorescence intensity in subphase and at interface is comparable.

The predicted sigmoidal behavior of $CtxB_5$ binding to the lipid monolayer by Hill equation (Shi et al, 2007) it's not easily observed in the case of this study. This might be caused by high standard deviation associated with measurements (fig. 19) – not only is the protein distribution in the monolayer during a single titration not homogeneous, but also there is a high degree of variability associated with independent samples. Various factors could contribute in the inhomogeneity of APD signal within a sample – firstly, protein clusters may form when it interacts with the lipid interface; secondly, the presence of meniscus in the lipid monolayer or other variations in the lipid packing which appear during lipid solution deposition

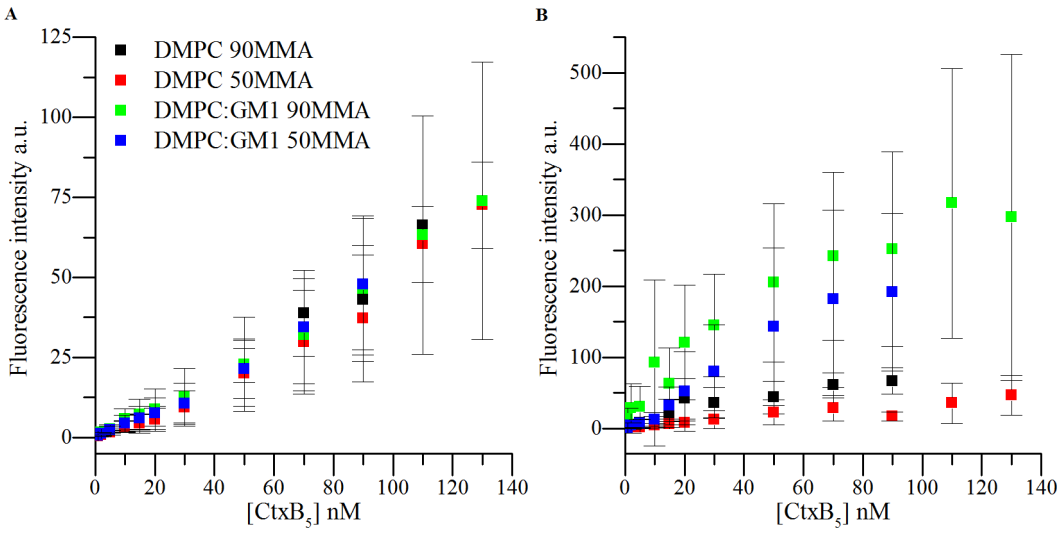

Fig. 18: Representative trends of subphase (*A*) and interface (*B*) $CtxB_5$-Alexa 647 fluorescence intensity in DMPC monolayers with different G_{M1} content (0 and 0.1 mol %) at 50 and 90 *MMA*. The means of independent samples (3-5) are represented with corresponding standard deviations.

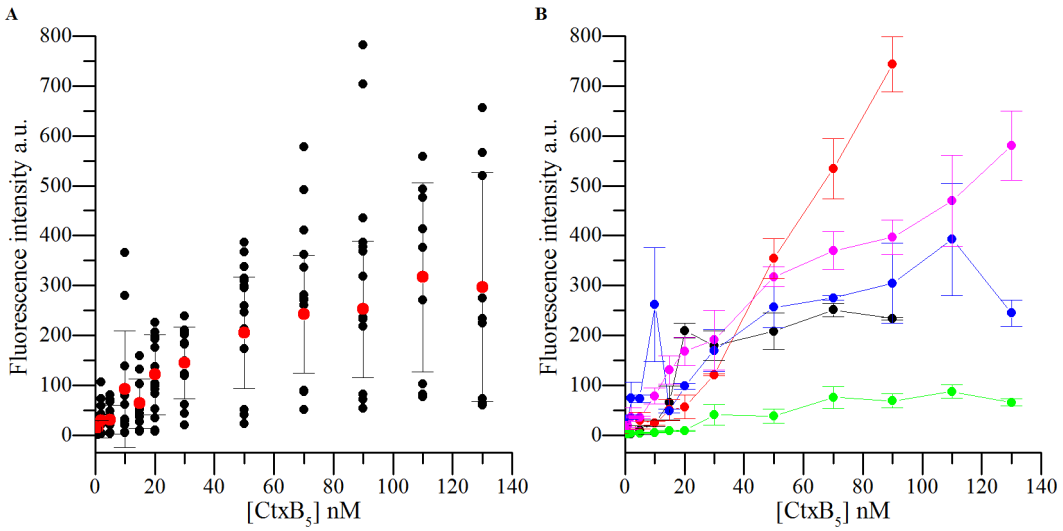

Fig. 19: *A.* Representative scattered graph of $CtxB_5$-Alexa 647 binding to DMPC monolayer containing 0.1 mol % G_{M1} at 90 *MMA*. The means (red) and corresponding deviations are also represented. *B.* Trends of independent measurements of $CtxB_5$-Alexa 647 binding to DMPC monolayer containing 0.1 mol % G_{M1} at 90 *MMA*.

at the interface could also alter protein binding to the monolayer. Furthermore, there are several factors that are still not fully controlled and thus vary between independent samples such as subphase evaporation, lipid oxidation or protein deposition at the glass cover slip. Thus, the data do not allow relevant fit and no reproducible trends or quantitative conclusions about protein binding can be obtained (fig. 19). Some of these concerned could be addressed by using a ROS (reactive oxygen species) scavenger in order to reduce lipid oxidation or by modifying chamber structure and treatment for a better control of subphase evaporation and protein deposition.

* 3.3. PROTEIN BINDING TO PHASE SEPARATED MONOLAYERS WITH DIFFERENT G_{M1} CONTENT

Based on $CtxB_5$ binding trend with lipid packing on homogeneous DMPC monolayers and differential G_{M1} partitioning suggested by literature (see below), a comparative study of its behavior in phase separated DOPC:bSM:Chol 1:1:1 monolayers with different G_{M1} content –0, 0.1 and 1 mol % was conducted (fig. 20). Lipid monolayers were imaged through confocal microscopy at each step of protein titration (till a maximum concentration of 130 nM) and, in order to proceed to a semi-quantitative analysis, fluorescence intensity profiles of representative cross-sections were taken (fig. 20).

Further image analysis allowed to assess mean $CtxB_5$ fluorescence intensity separately in LE and LC phase and to quantify the relative binding of the protein in these phases (fig. 21).

In absence of G_{M1}, $CtxB_5$ binds preferentially to the LE phase (fig. 21.*A*) as expected from earlier studies (Chwastek & Schwille, 2013) and previously presented results (fig. 17). Moreover, protein partitioning is dependent on the initial protein concentration – the ratio of fluorescence intensities between LE and LC phase increases with the concentration (fig. 21.*C*) as lipid binding curves suggest (fig. 17). Note that this behavior is apparently not reverted even at high protein concentration. When a small concentration of G_{M1} (0.1 mol %) is incorporated in the monolayer, there is no significant difference between $CtxB_5$ binding to LE or LC phase. Nonetheless, at low protein concentration (bellow 30 nM), $CtxB_5$ is enriched in LC phase as compared to LE phase (fig. 21.*B* and *C*) as expected from closely related work (Chwastek & Schwille, 2013), due to preferential incorporation of G_{M1} in ordered domains (Rock et al, 1991; Vié et al, 1998; Yuan & Johnston, 2000; Menke et al, 2002). As the available G_{M1} for binding is easily saturated, this tendency is reversed and LE phase show an increased $CtxB_5$ binding when compared to LC phase at total protein concentrations higher than 30 nM. On the other hand, when G_{M1} concentration in the monolayer is increased to 1 mol % the $CtxB_5$ enrichment in LC phase as compared to LE phase is stabilized (fig.20) as G_{M1} saturation is not reached in the range of analyzed protein concentrations (1 – 130 nM). Moreover, this trend is even more obvious as the initial protein concentration increases –at higher protein concentrations the laser power used during the imaging (generally kept at 5 %) was reduced to avoid channel saturation (0.2 %).

Thus, these results suggest that phase separation might be a mechanism of controlling protein-membrane interactions through differences in protein packing, as had already been shown in streptavidin experiments (fig. 9). Additionally, the roles of protein concentration (Phillips et al, 1975; Fidelio et al, 1981; Cumar et al, 1982) and membrane G_{M1} content (Shi et al, 2007) in CtxB binding are also confirmed.

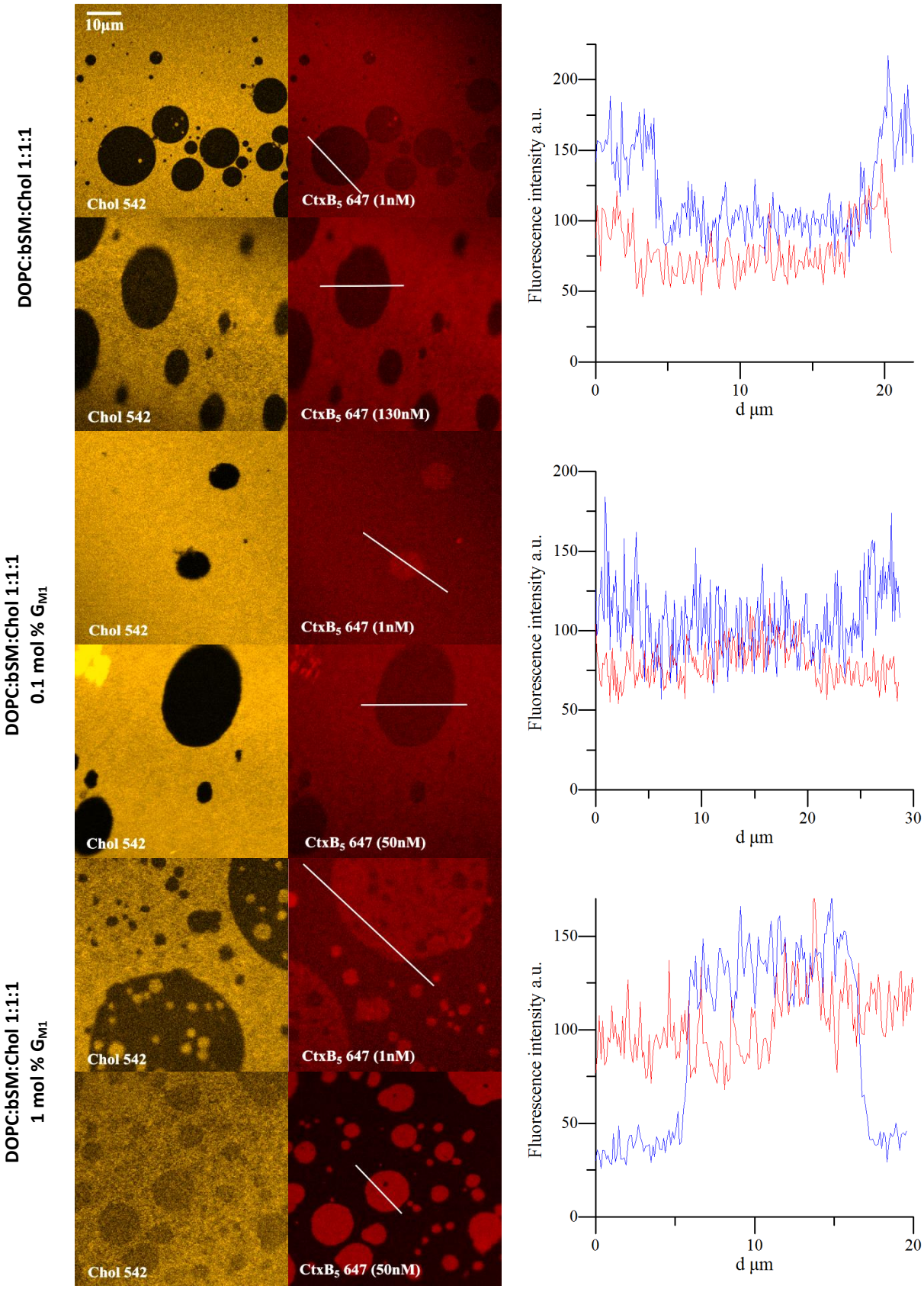

Fig. 20: Representative images of $CtxB_5$-Alexa 647 titration on DOPC:bSM:Chol 1:1:1 phase separated monolayers containing 0 (*A*), 0.1 (*B*) and 1 (*C*) mol % G_{M1}. Fluorescence intensity profiles of marked cross-sections are shown –1 nM (red) and 50/130 nM (blue) $CtxB_5$. Note that in the last pair of images laser power of protein channel was decreased 40x times to avoid channel saturation.

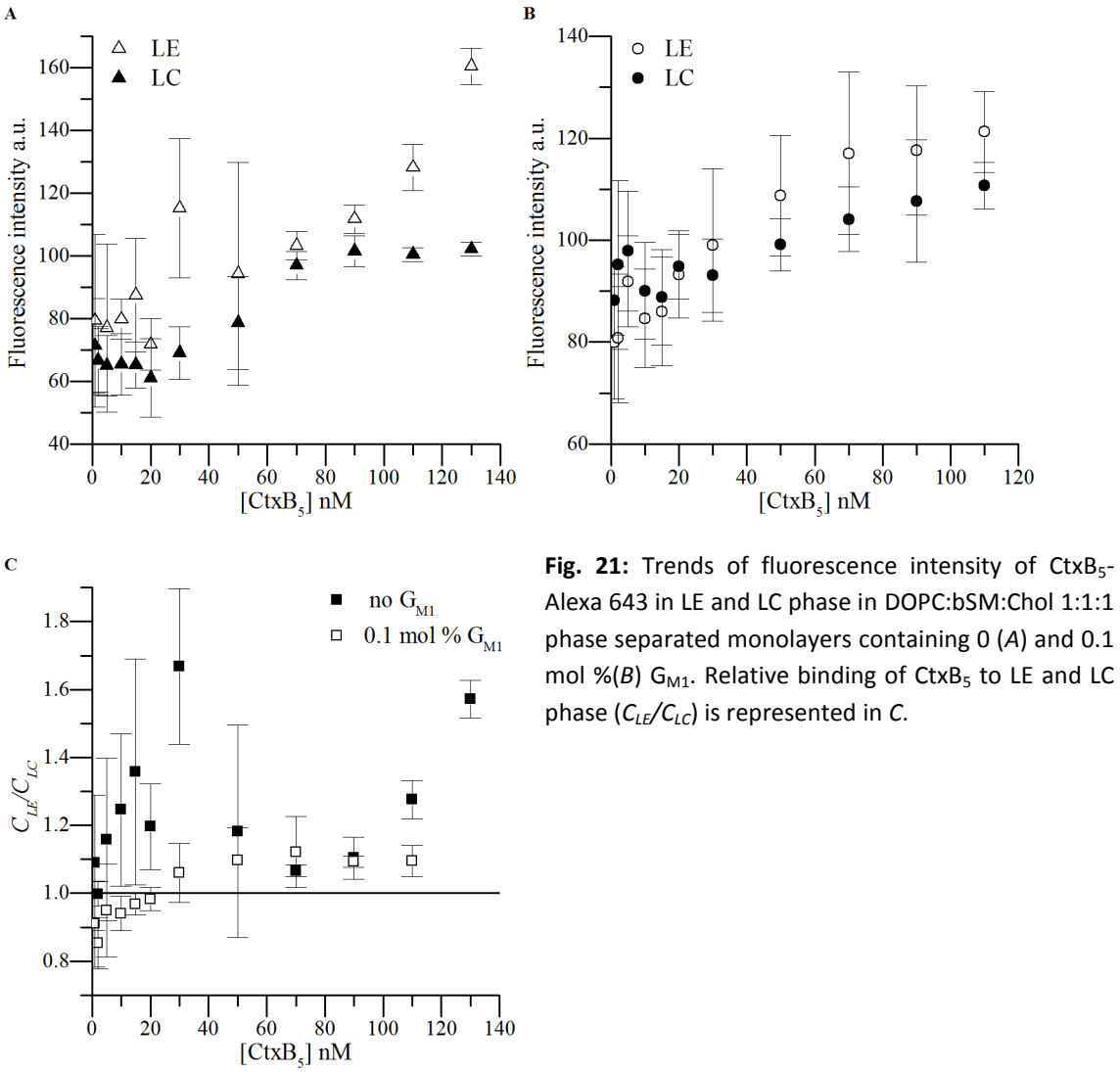

Fig. 21: Trends of fluorescence intensity of $CtxB_5$-Alexa 643 in LE and LC phase in DOPC:bSM:Chol 1:1:1 phase separated monolayers containing 0 (*A*) and 0.1 mol %(*B*) G_{M1}. Relative binding of $CtxB_5$ to LE and LC phase (C_{LE}/C_{LC}) is represented in *C*.

4. CONCLUSIONS

* 4.1. LIPID MONOLAYER CHARACTERIZATION

The developed miniaturized trough is shown to allow for robust characterization of morphology and mobility of monolayers. More specifically, monolayer homogeneity measurements at the studied *MMA* were accompanied by FCS assay which revealed a linear tendency of diffusion coefficients as a function of lipid density, as expected from the free area model proposed by Galla et al. in 1979. Moreover, the obtained *ac* values for DMPC (36.2 ± 4.72 / 37.2 ± 13.75 $Å^2$ in samples with different labels) are in good agreement with the literature. Nevertheless some deviations are expected at extreme lipid densities (50 and 100 *MMA*) as small variations in lipid deposition result in great lipid packing differences – formation of S and G phases respectively, which will influence the monolayer mobility.

* 4.2. PROTEIN-MONOLAYER BINDING

For both proteins, the results uncover the influence of lipid packing, and thus of lipid mobility and π, on protein binding – streptavidin and $CtxB_5$ bind stronger to the membrane at low lipid densities and, accordingly, low π and high lipid mobility. Although streptavidin appears to bind

stronger to lipid monolayers, $CtxB_5$ present a stronger surface activity as its binding to clean buffer-air interface is higher. Moreover, phase separated mixtures illustrate this behavior – proteins show higher affinity for loose LE phase then for tightly packed LC domains. Nonetheless, the surface non-active protein streptavidin tends to accumulate in the domain boundaries when the difference in lipid organization between domains is very high– for example in LE/S phase separations. Furthermore, titration experiments with $CtxB_5$ support this result as at 90 *MMA* the interface protein intensity is higher than at 50 *MMA*. Interestingly, these results confirm predictions made four decades ago through surface pressure variation study of different lipid monolayers on protein addition (Phillips et al, 1975; Fidelio et al, 1981; Cumar et al, 1982).

A specific binding could be obtained for $CtxB_5$ only by incorporation of G_{M1} in the monolayer. Although binding curves do not show it clearly, titration experiments reveal that the presence of 0.1 mol % G_{M1} is enough to highly increase protein binding to the monolayer. Also, the previously observed influence of lipid density is retained in presence of a specific ligand. However, in phase separated mixtures containing G_{M1}, protein binds preferentially to LC domains, as the ganglioside is preferentially distributed in these rigid domains (Rock et al, 1991; Vié et al, 1998; Yuan & Johnston, 2000; Menke et al, 2002).

Besides the influences of lipid packing and presence of ligand, it was also shown that the pool of available protein have an impact on the obtained results, in accordance with previous studies (Phillips et al, 1975; Fidelio et al, 1981; Cumar et al, 1982). This could be mediated by both the protein concentration and the ratio between available surface area and protein volume.

FINAL REMARKS

Protein-lipid interactions are one of the major focuses of membrane research as they play a central role in membrane organization, metabolism and signaling processes. Although a possible influence of lipid packing on protein binding to lipid layers had been proposed four decades ago (Phillips et al, 1975; Fidelio et al, 1981; Cumar et al, 1982), the methods available at the time were not enough to prove it.

Lipid monolayer is a classical model system which has been rather neglected in recent membrane research, even though it allows easy manipulation oflipid packing. Here, it is shown that despite its simplicity, the assay can be used to address current challenging biological problems, by convenient coupling with high resolution and high sensitivity techniques, such as confocal microscopy and FCS.

The miniaturized trough recently developed by Chwastek and Schwille is shown here to allow the deposition of monolayers with highly robust morphological and lipid mobility characteristics. Due to its reproducibility, low volume and technical versatility, the applied system can be easily used in protein binding assays. Two well-characterized proteins – streptavidin and $CtxB_5$ – were chosen for the validation of the proposed method, based on protein fluorescence measurement at both monolayer interface and subphase.

Here, by using this system in a semi-quantitative way, new evidence of the importance of lipid packing in protein-membrane interaction is achieved. It is shown that proteins easily penetrate the monolayer at low lipid densities, while at high π, the interaction is reduced. Phase separation serves as a mechanism of regulation of protein binding regulation not only through differential lipid packing but also ligand segregation. In addition, protein pool and available surface affect the binding as a function of protein concentration.

The presented system provides a powerful alternative approach to study protein-membrane interactions, allowing tuning of membrane parameters as lipid packing, which cannot be easily regulated in bilayers. The robust combination with confocal microscopy and spectroscopy, not only results in a high temporal resolution of particle mobility, but also achieves high spatial resolution in an assay. Altogether, the presented work was the first attempt to develop fluorescence-based quantitative assay which could be used to monitor binding of the protein to lipid monolayers.

FUTURE PERSPECTIVES

Despite the robustness of the method when applied to lipid analyses, some problems remain to be solved – the lipid probes do not distribute homogeneously in the monolayer. Thus, at increasing π one does not observe a consistent increase in the number of molecules in the V_{eff}. It is possible that at high surface pressures probe K_p between the water subphase and the monolayer is decreased, resulting in its partial exclusion from the monolayer. On the other hand, the increase in lipid density can increase weak interactions between different particles, resulting in dye clustering. Thus, further studies are needed to understand fluorophore behavior in lipid monolayers.

A better characterization of $CtxB_5$ and streptavidin unspecific binding to monolayers remain to be done. The nature of protein interaction with lipids can be further studied by manipulation of buffer conditions (e.g. salt content and concentration, pH). Also, variation of the amount of the ligand in the monolayer can give new insight into ligand-protein interactions. For streptavidin, in order to study its specific binding to monolayer surface, one could substitute streptavidin for the mutant form ExtrAvidin or Neutravidin which have shown better results in lipid bilayers.

Additionally, accurate protein binding quantification and K_D determination was not yet achieved. The high standard deviations associated to the binding assays seem to be related to a non-homogeneous incorporation of the protein in the lipid monolayer. Some of the error might originate from meniscus formation and discrepancies introduced during monolayer deposition and protein addition. Thus further standardization of applied lipid and protein solution volume, concentration and condition should be done.

Further, additional factors such as lipid oxidation, subphase evaporation and π difference are neither monitored nor controlled here. The use of a ROS scavenger system added to the subphase could help to reduce lipid oxidation, even though the hydrophobic carbon tails are pointed towards the air. Also, the creations of a tiny well around the chamber would allow for a better sample sealing when filled with water, helping to control evaporation. Due to the small chamber size the use of a Wilhelmy plate for π monitoring is hindered. Nonetheless, it is possible to calculate π through physical wave formation and its decay analysis.

In future, it is expected to get a more complete and quantified characterization of streptavidin and Ctx binding to lipid monolayers; particularly, the influences of lipid packing and ligand content. For example, the application of fluorescence cross-correlation spectroscopy (FCCS) technique could provide a more concrete analysis of specific interaction between the protein and its ligand. Ultimately, monolayers have the potential to provide a quantitative protein binding assay, which would be easily applied for other biologically relevant proteins – such as FCHo2, an F-BAR protein responsible for sensing and inducing membrane curvature.

SYMBOLS AND ABBREVIATIONS

π	Surface pressure
A	Area
ac	Critical point
APD	Avalanche photo diode
BAR	Bin-Amphiphysin-Rvs domain
bSM	Sphingomyelin
C_{inter}	Fluorescence signal at the interface
C_{sub}	Fluorescence signal at the subphase
Chol	Cholesterol
Chol 542	Cholesteryl 4,4-difluoro-5-(4-methoxyphenyl)-4-bora-3a,4a-diaza-*s*-indacene-3-undecanoate
Ctx	Cholera toxin
$CtxB_5$	Pentameric ring of cholera toxin subunit *B*
D	Diffusion coefficient
D_{non}	Rate of non-radiative energy dissipation
D_r	Rate of radiative energy dissipation
DiO	3,3'-dilinoleyloxacarbocyanine perchlorate
DMPC	1,2-dimyristoyl-*sn*-glycero-3-phosphocholine
DOPC	1,2-dioleoyl-*sn*-glycero-3-phosphocholine
DOPE-PEG350	1,2-dioleoyl-*sn*-glycero-3-phosphoethanolamine-N-[methoxy(polyethylene glycol)-350]
DPPC	1,2-dipalmitoyl-*sn*-glycero-3-phosphocholine
DPPE-Ncap-Biotin	1,2-dipalmitoyl-*sn*-glycero-3-phosphoethanolamine-N-(cap biotinyl)
DSPC	1,2-distearoyl-*sn*-glycero-3-phosphocholine
DSPE-PEG2000-Biotin	1,2-distearoyl-*sn*-glycero-3-phosphoethanolamine-N-[biotinyl(polyethylene glycol)-2000]
FAM	Free area model
FCS	Fluorescence correlation spectroscopy
$G(\tau)$	Autocorrelation function of fluorescence signal over time
G	Gas phase
G_{M1}	Ganglioside G_{M1}
GPMV	Giant plasma membrane vesicle
GUV	Giant unilamelar vesicle
IC	Internal conversion
ICC	Intersystem crossing conversion
K_D	Dissociation constant

K_P	Partition coefficient
l_d	Liquid disordered phase
l_o	Liquid ordered phase
LC	Liquid condensed phase
LE	Liquid expanded phase
MMA	Mean molecular area
N	Number of particles
Q	Quantum yield
S	Solid phase
SLB	Supported lipid bilayer
r_0	Waist of the focal spot
T_m	Phase transition temperature
V_{eff}	Effective focal volume or detection volume
w/w	Mass fraction (weight/weight)

REFERENCES

Allen C, Dos Santos N, Gallagher R, Chiu GN, Shu Y, Li WM, Johnstone SA, Janoff AS, Mayer LD, Webb MS, Bally MB (2002) Controlling the physical behavior and biological performance of liposome formulations through use of surface grafted poly(ethylene glycol). *Bioscience reports* **22:** 225-250

Angelova MI, Dimitrov DS (1986) Liposome Electroformation. *Faraday Discussions* **81:** 303-+

Arumugam S, Chwastek G, Schwille P (2011) Protein-membrane interactions: the virtue of minimal systems in systems biology. *Wiley Interdiscip Rev Syst Biol Med* **3:** 269-280

Auguste DT, Kirkwood J, Kohn J, Fuller GG, Prud'homme RK (2008) Surface rheology of hydrophobically modified PEG polymers associating with a phospholipid monolayer at the air-water interface. *Langmuir* **24:** 4056-4064

Baekmark TR, Elender G, Lasic DD, Sackmann E (1995) Conformational transtitions of mixed monolayers of phospholipids and poly(ethylene oxide) lipopolymers and interaction forces with solid surfaces. *Langmuir* **11:** 3975-3987

Bagatolli LA, Gratton E (2000) Two photon fluorescence microscopy of coexisting lipid domains in giant unilamellar vesicles of binary phospholipid mixtures. *Biophysical journal* **78:** 290-305

Bianco ID, Fidelio GD, Maggio B (1989) Modulation of phospholipase A2 activity by neutral and anionic glycosphingolipids in monolayers. *The Biochemical journal* **258:** 95-99

Brockman H (1999) Lipid monolayers: why use half a membrane to characterize protein-membrane interactions? *Curr Opin Struct Biol* **9:** 438-443

Chaiet L, Wolf FJ (1964) The Properties of Streptavidin, a Biotin-Binding Protein Produced by Streptomycetes. *Arch Biochem Biophys* **106:** 1-5

Chiantia S, Ries J, Kahya N, Schwille P (2006) Combined AFM and two-focus SFCS study of raft-exhibiting model membranes. *Chemphyschem : a European journal of chemical physics and physical chemistry* **7:** 2409-2418

Chiantia S, Ries J, Schwille P (2009) Fluorescence correlation spectroscopy in membrane structure elucidation. *Biochimica et biophysica acta* **1788:** 225-233

Chwastek G (2013) Interactions of FCHo2 with lipid membranes. Doctor Thesis, Faculty of Mathematics and Natural Sciences, Dresden University of Technology

Chwastek G, Schwille P (2013) A monolayer assay tailored to investigate lipid-protein systems. *Chemphyschem : a European journal of chemical physics and physical chemistry* **14:** 1877-1881

Claxton NS, Fellers TJ, Davidson MW (2005) Laser Scanning Confocal Microscopy. *Unpublished*

Cumar FA, Maggio B, Caputto R (1982) Ganglioside-cholera toxin interactions: a binding and lipid monolayer study. *Molecular and cellular biochemistry* **46:** 155-160

de Almeida RFM, Loura LM, Fedorov A, Prieto M (2005) Lipid rafts have different sizes depending on membrane composition: a time-resolved fluorescence resonance energy transfer study. *Journal of molecular biology* **346:** 1109-1120

de Almeida RFM, Loura LMS (2004) *Tópicos de Biofísica de Membranas*, Portugal.

Diamandis EP, Christopoulos TK (1991) The biotin-(strept)avidin system: principles and applications in biotechnology. *Clin Chem* **37:** 625-636

Dynarowicz-Latka P, Dhanabalan A, Oliveira ON, Jr. (2001) Modern physicochemical research on Langmuir monolayers. *Adv Colloid Interface Sci* **91:** 221-293

Fidelio GD, Maggio B, Cumar FA, Caputto R (1981) Interaction of glycosphingolipids with melittin and myelin basis protein in monolayers. *The Biochemical journal* **193:** 643-646

Fishman PH, Moss J, Osborne JC, Jr. (1978) Interaction of choleragen with the oligosaccharide of ganglioside GM1: evidence for multiple oligosaccharide binding sites. *Biochemistry* **17:** 711-716

Ford MG, Pearse BM, Higgins MK, Vallis Y, Owen DJ, Gibson A, Hopkins CR, Evans PR, McMahon HT (2001) Simultaneous binding of PtdIns(4,5)P2 and clathrin by AP180 in the nucleation of clathrin lattices on membranes. *Science (New York, NY)* **291:** 1051-1055

Franquelim HG (2012) The role of lipid membranes in the mechanism of action of sifuvirtide and other HIV-1 fusion inhibitors. Doctor Thesis, Faculty of Medicine, Univeristy of Lisbon

Franquelim HG, Veiga AS, Weissmuller G, Santos NC, Castanho MA (2010) Unravelling the molecular basis of the selectivity of the HIV-1 fusion inhibitor sifuvirtide towards phosphatidylcholine-rich rigid membranes. *Biochimica et biophysica acta* **1798:** 1234-1243

Galla HJ, Hartmann W, Theilen U, Sackmann E (1979) On two-dimensional passive random walk in lipid bilayers and fluid pathways in biomembranes. *J Membr Biol* **48:** 215-236

Gallop JL, Jao CC, Kent HM, Butler PJ, Evans PR, Langen R, McMahon HT (2006) Mechanism of endophilin N-BAR domain-mediated membrane curvature. *The EMBO journal* **25:** 2898-2910

Galloway TS, van Heyningen S (1987) Binding of NAD+ by cholera toxin. *The Biochemical journal* **244:** 225-230

Gaullier JM, Simonsen A, D'Arrigo A, Bremnes B, Stenmark H, Aasland R (1998) FYVE fingers bind PtdIns(3)P. *Nature* **394:** 432-433

Gennis RB (1989) *Biomembranes - molecular structure and function*, 1st edn. New York.

Georgiev GA, Sarker DK, Al-Hanbali O, Georgiev GD, Lalchev Z (2007) Effects of poly (ethylene glycol) chains conformational transition on the properties of mixed DMPC/DMPE-PEG thin liquid films and monolayers. *Colloids and surfaces B, Biointerfaces* **59:** 184-193

Gorter E, Grendel F (1925) ON BIMOLECULAR LAYERS OF LIPOIDS ON THE CHROMOCYTES OF THE BLOOD. *The Journal of experimental medicine* **41:** 439-443

Gudmand M, Fidorra M, Bjornholm T, Heimburg T (2009) Diffusion and partitioning of fluorescent lipid probes in phospholipid monolayers. *Biophysical journal* **96:** 4598-4609

Heinemann F, Vogel SK, Schwille P (2013) Lateral membrane diffusion modulated by a minimal actin cortex. *Biophysical journal* **104:** 1465-1475

Hendrickson WA, Pahler A, Smith JL, Satow Y, Merritt EA, Phizackerley RP (1989) Crystal structure of core streptavidin determined from multiwavelength anomalous diffraction of

synchrotron radiation. *Proceedings of the National Academy of Sciences of the United States of America* **86:** 2190-2194

Henne WM, Kent HM, Ford MG, Hegde BG, Daumke O, Butler PJ, Mittal R, Langen R, Evans PR, McMahon HT (2007) Structure and analysis of FCHo2 F-BAR domain: a dimerizing and membrane recruitment module that effects membrane curvature. *Structure* **15:** 839-852

Herold C, Chwastek G, Schwille P, Petrov EP (2012) Efficient electroformation of supergiant unilamellar vesicles containing cationic lipids on ITO-coated electrodes. *Langmuir* **28:** 5518-5521

Holmgren J (1981) Actions of cholera toxin and the prevention and treatment of cholera. *Nature* **292:** 413-417

Hyre DE, Le Trong I, Merritt EA, Eccleston JF, Green NM, Stenkamp RE, Stayton PS (2006) Cooperative hydrogen bond interactions in the streptavidin-biotin system. *Protein Science* **15:** 459-467

Kahya N, Scherfeld D, Bacia K, Poolman B, Schwille P (2003) Probing lipid mobility of raft-exhibiting model membranes by fluorescence correlation spectroscopy. *J Biol Chem* **278:** 28109-28115

Kastrup L, Blom H, Eggeling C, Hell SW (2005) Fluorescence fluctuation spectroscopy in subdiffraction focal volumes. *Physical review letters* **94:** 178104

Khmelinskaia A, Ibarguren M, de Almeida RFM, López DJ, A. PV, Ahayayauch H, Goñi FM, Escriba P (2013) Membrane order and hydration changes upon spontaneous insertion of 2-hydroxylated unsaturated fatty acids in the lipid bilayer. *In preparation*

Kim K, Kim C, Byun Y (2000) Preparation of a PEG-grafted phospholipid Langmuir-Blodgett monolayer for blood-compatible material. *J Biomed Mater Res* **52:** 836-840

Kim K, Kim C, Byun Y (2001) Preparation od a dipalmitoylphosphaticylcholine/cholesterol langmuir-blodgett monolayer that suppresses protein adsorption. *Langmuir* **17:** 5066-5070

Koynova R, Caffrey M (1998) Phases and phase transitions of the phosphatidylcholines. *Biochimica et biophysica acta* **1376:** 91-145

Kycia AH, Wang J, Merrill AR, Lipkowski J (2011) Atomic force microscopy studies of a floating-bilayer lipid membrane on a Au(111) surface modified with a hydrophilic monolayer. *Langmuir* **27:** 10867-10877

Laitinen OH, Nordlund HR, Hytonen VP, Kulomaa MS (2007) Brave new (strept)avidins in biotechnology. *Trends Biotechnol* **25:** 269-277

Lakowicz JR (2006) *Principles of Fluorescence Spectroscopy*, 3rd edn. Singapore.

Lichte B, Veh RW, Meyer HE, Kilimann MW (1992) Amphiphysin, a novel protein associated with synaptic vesicles. *The EMBO journal* **11:** 2521-2530

Livnah O, Bayer EA, Wilchek M, Sussman JL (1993) The structure of the complex between avidin and the dye, 2-(4'-hydroxyazobenzene) benzoic acid (HABA). *FEBS letters* **328:** 165-168

Ludwig DS, Ribi HO, Schoolnik GK, Kornberg RD (1986) Two-dimensional crystals of cholera toxin B-subunit-receptor complexes: projected structure at 17-A resolution. *Proceedings of the National Academy of Sciences of the United States of America* **83:** 8585-8588

Manna D, Albanese A, Park WS, Cho W (2007) Mechanistic basis of differential cellular responses of phosphatidylinositol 3,4-bisphosphate- and phosphatidylinositol 3,4,5-trisphosphate-binding pleckstrin homology domains. *J Biol Chem* **282:** 32093-32105

Martin P, Szablewski M (2004) *Langmuir-blodgett troughs - operating manual*, 6th edn. England.

McConnell HM, Tamm LK, Weis RM (1984) Periodic structures in lipid monolayer phase transitions. *Proceedings of the National Academy of Sciences of the United States of America* **81:** 3249-3253

Mekalanos JJ, Collier RJ, Romig WR (1979) Enzymic activity of cholera toxin. II. Relationships to proteolytic processing, disulfide bond reduction, and subunit composition. *J Biol Chem* **254:** 5855-5861

Menke M, Kunneke S, Janshoff A (2002) Lateral organization of GM1 in phase-separated monolayers visualized by scanning force microscopy. *European biophysics journal : EBJ* **31:** 317-322

Merkle D, Kahya N, Schwille P (2008) Reconstitution and anchoring of cytoskeleton inside giant unilamellar vesicles. *Chembiochem* **9:** 2673-2681

Middlebrook JL, Dorland RB (1984) Bacterial Toxins - Cellular Mechanisms of Action. *Microbiological Reviews* **48:** 199-221

Nelson DL, Cox MM (2004) *Lehninger Principles of Biochemistry*, 3rd edn. New York.

Nordlund HR, Hytonen VP, Laitinen OH, Uotila ST, Niskanen EA, Savolainen J, Porkka E, Kulomaa MS (2003) Introduction of histidine residues into avidin subunit interfaces allows pH-dependent regulation of quaternary structure and biotin binding. *FEBS letters* **555:** 449-454

Nuscher B, Kamp F, Mehnert T, Odoy S, Haass C, Kahle PJ, Beyer K (2004) Alpha-synuclein has a high affinity for packing defects in a bilayer membrane: a thermodynamics study. *The Journal of biological chemistry* **279:** 21966-21975

Peterson JW, Ochoa LG (1989) Role of prostaglandins and cAMP in the secretory effects of cholera toxin. *Science (New York, NY)* **245:** 857-859

Petrasek Z, Schwille P (2008) Precise measurement of diffusion coefficients using scanning fluorescence correlation spectroscopy. *Biophysical journal* **94:** 1437-1448

Petrov EP, Schwille P (2008) Translational diffusion in lipid membranes beyond the Saffman-Delbruck approximation. *Biophysical journal* **94:** L41-43

Phillips MC, Chapman D (1968) Monolayer characteristics of saturated 1,2,-diacyl phosphatidylcholines (lecithins) and phosphatidylethanolamines at the air-water interface. *Biochimica et biophysica acta* **163:** 301-313

Phillips MC, Hauser H, Leslie RB, Oldani D (1975) A comparison of the interfacial interactions of the apoprotein from high density lipoprotein and beta-casein with phospholipids. *Biochimica et biophysica acta* **406:** 402-414

Reed RA, Mattai J, Shipley GG (1987) Interaction of cholera toxin with ganglioside GM1 receptors in supported lipid monolayers. *Biochemistry* **26:** 824-832

Rex S, Zuckermann MJ, Lafleur M, Silvius JR (1998) Experimental and Monte Carlo simulation studies of the thermodynamics of polyethyleneglycol chains grafted to lipid bilayers. *Biophysical journal* **75:** 2900-2914

Rigler R, Pramanik A, Jonasson P, Kratz G, Jansson OT, Nygren P, Stahl S, Ekberg K, Johansson B, Uhlen S, Uhlen M, Jornvall H, Wahren J (1999) Specific binding of proinsulin C-peptide to human cell membranes. *Proceedings of the National Academy of Sciences of the United States of America* **96:** 13318-13323

Ringemann C, Harke B, von Middendorff C, Medda R, Honigmann A, Wagner R, Leutenegger M, Schonle A, Hell SW, Eggeling C (2009) Exploring single-molecule dynamics with fluorescence nanoscopy. *New Journal of Physics* **11**

Rock P, Allietta M, Young WW, Jr., Thompson TE, Tillack TW (1991) Ganglioside GM1 and asialo-GM1 at low concentration are preferentially incorporated into the gel phase in two-component, two-phase phosphatidylcholine bilayers. *Biochemistry* **30:** 19-25

Sabatini K, Mattila JP, Kinnunen PK (2008) Interfacial behavior of cholesterol, ergosterol, and lanosterol in mixtures with DPPC and DMPC. *Biophysical journal* **95:** 2340-2355

Sano T, Cantor CR (1995) Intersubunit contacts made by tryptophan 120 with biotin are essential for both strong biotin binding and biotin-induced tighter subunit association of streptavidin. *Proceedings of the National Academy of Sciences of the United States of America* **92:** 3180-3184

Sarmento MJ, Prieto M, Fernandes F (2012) Reorganization of lipid domain distribution in giant unilamellar vesicles upon immobilization with different membrane tethers. *Biochimica et biophysica acta* **1818:** 2605-2615

Sattler J, Schwarzmann G, Knack I, Rohm KH, Wiegandt H (1978) Studies of ligand binding to cholera toxin, III. Cooperativity of oligosaccharide binding. *Hoppe Seylers Z Physiol Chem* **359:** 719-723

Schafer LV, Marrink SJ (2010) Partitioning of lipids at domain boundaries in model membranes. *Biophysical journal* **99:** L91-93

Schwille P, Haustein E. (2002) Fluorescence Correlation Spectroscopy, *An Introduction to its Concepts and Applications*. In (BTOL) BTO (ed.),
http://www.biophysics.org/education/schwille.pdf

Schwille P, Kummer S, Heikal AA, Moerner WE, Webb WW (2000) Fluorescence correlation spectroscopy reveals fast optical excitation-driven intramolecular dynamics of yellow fluorescent proteins. *Proceedings of the National Academy of Sciences of the United States of America* **97:** 151-156

Shi J, Yang T, Kataoka S, Zhang Y, Diaz AJ, Cremer PS (2007) GM1 clustering inhibits cholera toxin binding in supported phospholipid membranes. *Journal of the American Chemical Society* **129:** 5954-5961

Simons K, Ikonen E (1997) Functional rafts in cell membranes. *Nature* **387:** 569-572;

Singer SJ, Nicolson GL (1972) The fluid mosaic model of the structure of cell membranes. *Science (New York, NY)* **175:** 720-731

Sorre B, Callan-Jones A, Manneville JB, Nassoy P, Joanny JF, Prost J, Goud B, Bassereau P (2009) Curvature-driven lipid sorting needs proximity to a demixing point and is aided by proteins. *Proceedings of the National Academy of Sciences of the United States of America* **106:** 5622-5626

Stefl M, Sachl R, Humpolickova J, Cebecauer M, Machan R, Kolarova M, Johansson LB, Hof M (2012) Dynamics and size of cross-linking-induced lipid nanodomains in model membranes. *Biophysical journal* **102:** 2104-2113

Stepniewski M, Pasenkiewicz-Gierula M, Rog T, Danne R, Orlowski A, Karttunen M, Urtti A, Yliperttula M, Vuorimaa E, Bunker A (2011) Study of PEGylated lipid layers as a model for PEGylated liposome surfaces: molecular dynamics simulation and Langmuir monolayer studies. *Langmuir* **27:** 7788-7798

Takai Y, Kishimoto A, Iwasa Y, Kawahara Y, Mori T, Nishizuka Y (1979) Calcium-Dependent Activation of a Multifunctional Protein-Kinase by Membrane Phospholipids. *Journal of Biological Chemistry* **254:** 3692-3695

Tamm LK, McConnell HM (1985) Supported phospholipid bilayers. *Biophysical journal* **47:** 105-113

Tanwir K, Tsoukanova V (2008) Lateral distribution of a poly(ethylene glycol)-grafted phospholipid in phosphocholine monolayers studied by epifluorescence microscopy. *Langmuir* **24:** 14078-14087

Tomasi M, Battistini A, Araco A, Roda LG, D'Agnolo G (1979) The role of the reactive disulfide bond in the interaction of cholera-toxin functional regions. *Eur J Biochem* **93:** 621-627

Tristram-Nagle S, Petrache HI, Nagle JF (1998) Structure and interactions of fully hydrated dioleoylphosphatidylcholine bilayers. *Biophysical journal* **75:** 917-925

Tsoukanova V, Salesse C (2008) Mixing behavior of a poly(ethylene glycol)-grafted phospholipid in monolayers at the air/water interface. *Langmuir* **24:** 13019-13029

Valeur B (2002) *Molecular fluorescence - principles and applications*, Federal Republic of Germany.

van Meer G, Voelker DR, Feigenson GW (2008) Membrane lipids: where they are and how they behave. *Nat Rev Mol Cell Biol* **9:** 112-124

Vié VvM, N., Lesniewska E, Goudonnet JP, Heitz F, le Grimellec C (1998) Distribution of Ganglioside GM1 between Two-Component, Two-Phase Phosphatidylcholine Monolayers. *Langmuir* **14:** 4574-4583

Vogel SK, Schwille P (2012) Minimal systems to study membrane-cytoskeleton interactions. *Current opinion in biotechnology* **23:** 758-765

Wilke N, Vega Mercado F, Maggio B (2010) Rheological properties of a two phase lipid monolayer at the air/water interface: effect of the composition of the mixture. *Langmuir* **26:** 11050-11059

Yarrow F, Kuipers BW (2011) AFM study of the thermotropic behaviour of supported DPPC bilayers with and without the model peptide WALP23. *Chemistry and physics of lipids* **164:** 9-15

Yuan C, Johnston LJ (2000) Distribution of ganglioside GM1 in L-alpha-dipalmitoylphosphatidylcholine/cholesterol monolayers: a model for lipid rafts. *Biophysical journal* **79:** 2768-2781

Yun H, Choi Y-W, Kim NJ, Sohn D (2003) Physicochemical properties of phosphatidylcholine (PC) monolayers with different alkyl chains, at the air/water interface. *Bull Korean Chem Soc* **24:** 377-383

Zhang RG, Scott DL, Westbrook ML, Nance S, Spangler BD, Shipley GG, Westbrook EM (1995) The three-dimensional crystal structure of cholera toxin. *Journal of molecular biology* **251:** 563-573.